Genetics Research

Identification of Genetic and Epigenetic Markers of Complex Diseases through Integrating Multiscale Biological Data

Lead Guest Editor: Jian-Xin Shi
Guest Editors: Chang Gu, Jun Yang, Xufeng Pan, Haoran Liu, and Dechen Zhang

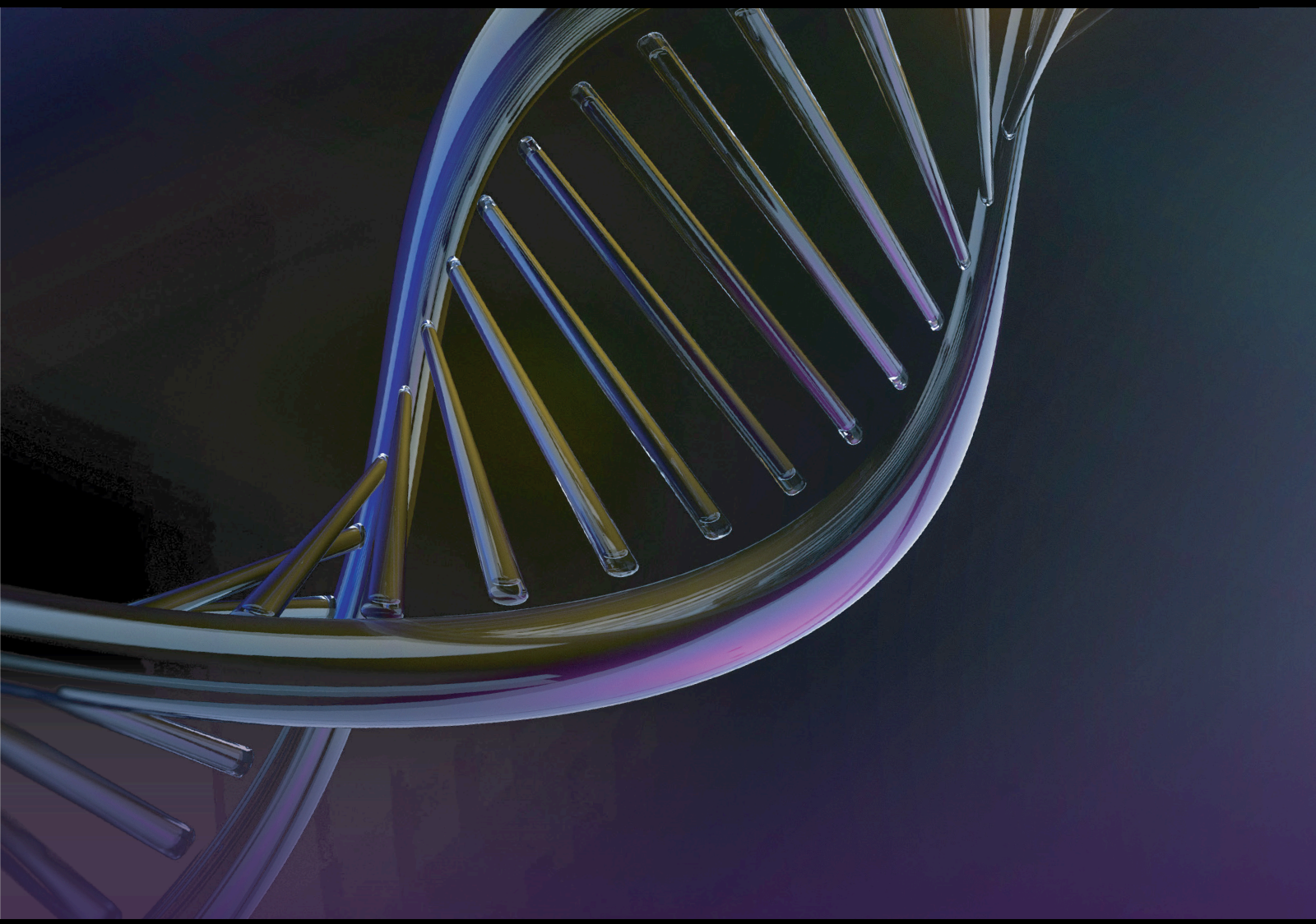

Identification of Genetic and Epigenetic Markers of Complex Diseases through Integrating Multiscale Biological Data

Genetics Research

Identification of Genetic and Epigenetic Markers of Complex Diseases through Integrating Multiscale Biological Data

Lead Guest Editor: Jian-Xin Shi
Guest Editors: Chang Gu, Jun Yang, Xufeng Pan, Haoran Liu, and Dechen Zhang

Academic Editors

Contents

Hindawi
Genetics Research
Volume 2022, Article ID 5896296, 13 pages
https://doi.org/10.1155/2022/5896296

CAMBRIDGE
UNIVERSITY PRESS

Research Article

Transcriptome Sequencing Analysis of the Effect of β-Elemene on Colorectal Cancer from the lncRNA-miRNA-mRNA Perspective

Heng Deng,[1] **Shuo Chen**,[2] **Xiancang Yuan**,[3] **and Jun Zhang**[4]

[1]*Department of Anorectal Surgery, Second Affiliated Hospital of Anhui University of Chinese Medicine, Hefei, China*
[2]*The Graduate School, Guangzhou University of Chinese Medicine, Guangzhou, China*
[3]*Department of Anorectal Surgery, Huainan City First People's Hospital, Huainan, China*
[4]*Chinese Medicine Teaching and Research Section, Anhui University of Chinese Medicine, Hefei, China*

Correspondence should be addressed to Jun Zhang; zhangjun98765432@163.com

Received 24 June 2022; Revised 18 August 2022; Accepted 22 August 2022; Published 13 September 2022

Academic Editor: Jun Yang

Object. β-Elemene is an emerging antitumor Chinese medicine, but the exact mechanism of action of β-elemene in colorectal cancer (CRC) remains unclear. This study aimed to explore the mechanism of the lncRNA-miRNA-mRNA network in the process of β-elemene inhibiting CRC. *Methods.* RNA sequencing was performed on CRC cells from the control group (untreated) and the case group (β-elemene-treated). According to the sequencing data, we screened the differentially expressed (DE) lncRNAs, miRNAs, and mRNAs and then analyzed them by functional enrichment analyses. Through the lncRNA-miRNA-mRNA network, the key miRNAs and mRNAs involved in the process of β-elemene inhibiting CRC were further identified. *Results.* Totally, 607 upregulated and 599 downregulated DElncRNAs, 12 downregulated and 24 upregulated DEmiRNAs, and 3153 downregulated and 3248 upregulated DEmRNAs were identified. Through the lncRNA-miRNA-mRNA network, 3 miRNAs (miR-7109-3p, miR-4506, and miR-3182), 7 prognostic mRNAs (ALPG, DTX1, HOXD13, RIMS3, SLC16A8, SYT1, and TNNT1), and 2 key mRNAs (RIMS3 and SLC16A8) were determined to participate in the inhibitory mechanism of β-elemene in CRC. *Conclusion.* This study revealed for the first time that the lncRNA-miRNA-mRNA network is involved in the regulation of β-elemene in CRC, and these identified miRNAs and mRNAs could be new clinical prognostic biomarkers and therapeutic targets for CRC patients.

1. Background

Colorectal cancer (CRC) is a kind of disease with an increased morbidity year by year [1]. Many factors may contribute to the incidence of CRC, including genetics, environment, colon polyp, diet habits, and so on [2, 3]. Bloody stool is usually the earliest and commonest symptom of CRC. When it comes to the advanced stage, there will be anemia, acute peritonitis, tumor metastasis, and so on [3, 4]. In the recent 50 years, although much progress has been made in medical conditions, the 5 years survival rate of CRC still hovers around 50% due to its high recurrence [5]. At present, it is still important to explore new, safe, and effective treatment options for CRC patients.

In recent years, studies have shown that RNA with different lengths interacts with each other, especially among microRNA (miRNA), long noncoding RNA (lncRNA), and messenger RNA (mRNA), thus forming a mutual regulatory network of lncRNA-miRNA-mRNA that is important to show the interactions between RNA molecules and explain their functions [6–8]. With relatively high specificity in cells and tissues and a wide existence in various human tissues from serum and stool, miRNAs are good noninvasive biological agents for the measurement of precancerous and cancerous lesions and therapeutic targets in many diseases [9, 10]. Thus, searching for miRNAs in CRC progression and its mRNA targets could be a method to find more effective diagnostic biomarkers and treatment targets for CRC

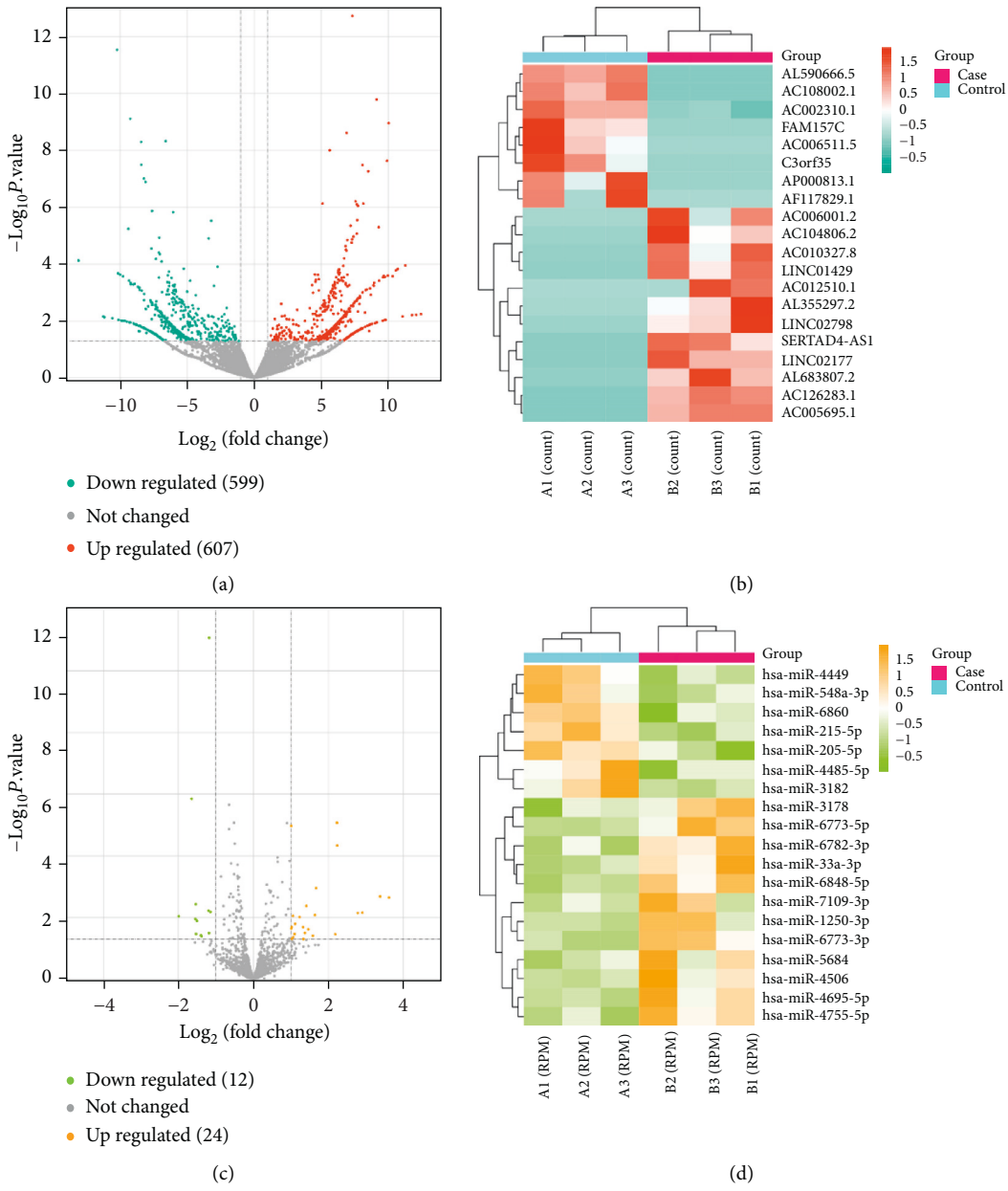

Figure 1: Continued.

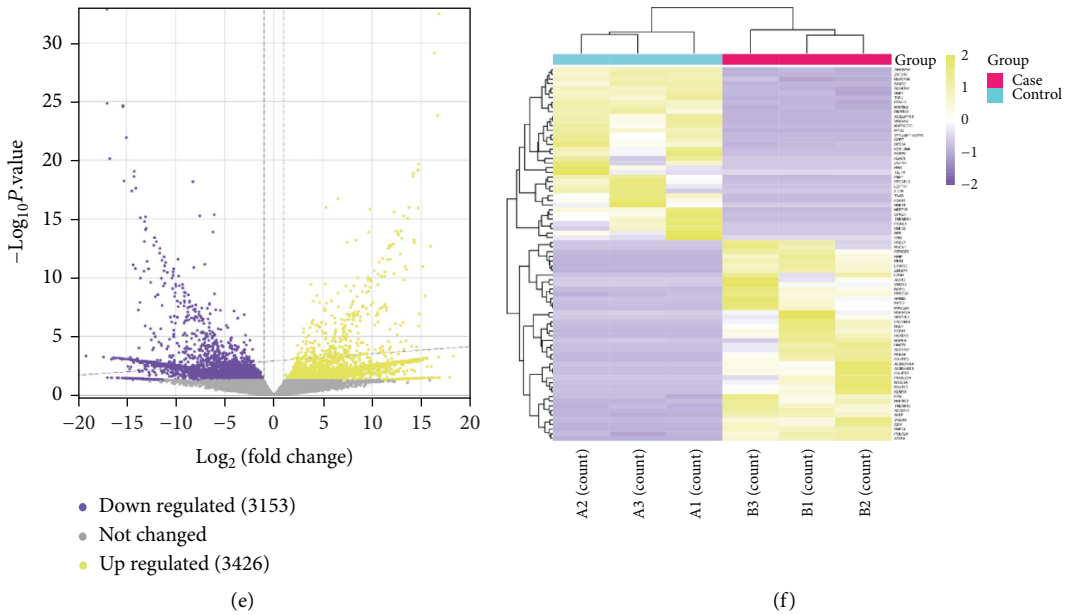

Figure 1: Identification of DElncRNA, DEmiRNA, and DEmRNA induced by β-elemene treatment in CRC. (a)-(b) Volcano map and heat map of lncRNAs. Blue stands for downregulated DEGs, red stands for upregulated DEGs, and gray stands for no significant change in genes. (c)-(d) Volcano map and heat map of miRNAs. Green stands for downregulated DEGs, orange stands for upregulated DEGs, and gray stands for no significant change in genes. (e)-(f) Volcano map and heat map of mRNAs. Yellow stands for downregulated DEGs, purple stands for upregulated DEGs, and gray stands for no significant change in genes.

patients. Previously, some researchers analyzed the correlation between abnormally expressed miRNAs and CRC by constructing a differential miRNA bioinformatics expression map and predicted that it would affect CRC by interfering with downstream signaling pathways [11].

β-Elemene is a bioactive compound extracted from natural plants. As an emerging antitumor Chinese medicine, β-elemene has been applied in medical therapies because it could boost the effects of other antitumor Chinese medicines on lung cancer [12], breast cancer [13], colorectal cancer [14], glioma [15], osteosarcoma [16], and so on and decrease the side effects of radiotherapy and chemotherapy [17]. Previously, Chen P et al. found that by triggering ferroptosis and suppressing EMT, the β-elemene and cetuximab therapies were sensitive to KRAS-mutated CRC cells [14]. The other report indicates that β-elemene could suppress the occurrence and development of CRC in the nude mouse by affecting transplanted tumor proliferation, apoptosis, and autophagy process [18]. However, the exact mechanism between β-elemene and CRC has not been studied yet. Therefore, we intend to analyze the regulatory lncRNA-miRNA-mRNA mechanism of β-elemene-miRNA-mRNA in CRC by whole quasi-transcriptome sequencing.

This study plans to investigate the mechanism of the lncRNA-miRNA-mRNA network in the process of β-elemene inhibiting CRC and to further find promising therapeutic targets and prognostic biomarkers for CRC. Our findings will bring a new perspective to the CRC study and lay the therapeutic basis for the clinical treatment of CRC patients.

2. Materials and Methods

2.1. Cell Culture and Treatment. The HCT-116 cells were from the China National Collection of Authenticated Cell Culture (Shanghai, China). The cells were cultured in Dulbecco's modified Eagle's medium (DMEM) obtained from Carlsbad, CA, USA, with 2 ml glutamine and 10% Fetal bovine serum (FBS) obtained from Gibco, USA, in a humidified environment with 5% CO_2 at 37°C. β-Elemene is available from Sigma. Cells treated with β-elemene were further used for RNA sequencing.

2.2. Small RNA Sequencing. We selected the control (no treatment) and case groups (β-elemene treatment) for RNA sequencing and pertinent analysis. Then, the RNA sequencing was performed by Origin-Biotech Inc. (Shanghai, China).

2.3. Identification of Differentially Expressed (DE) lncRNA, miRNA, and mRNA. Based on the RNA sequencing data, DElncRNA, DEmiRNA, and DEmRNA were identified by edgeR with a threshold of $P < 0.05$ and the absolute values of $|\log_2$ fold change (FC)$|>1$, respectively.

2.4. Functional Enrichment Analysis on the DElncRNA, DEmiRNA, and DEmRNA. Gene Ontology (GO) contains a set of related terms or concepts, and it describes the understanding of biology from three domains: cellular

Table 1: Top 5 increased and decreased DElncRNAs.

Gene ID	Transcript	Gene name	Status	*P* value
ENSG00000225791	ENST00000667019	TRAM2	Increased	1.12E-09
ENSG00000285517	ENST00000649390	Novel gene	Increased	2.35E-08
ENSG00000271853	ENST00000497086	Novel gene	Increased	5.04E-06
ENSG00000258525	ENST00000661204	Novel gene	Increased	1.64E-10
ENSG00000179818	ENST00000654878	PCBP1	Increased	5.46E-08
ENSG00000260528	ENST00000563357	FAM157 C	Decreased	3.20E-08
ENSG00000247679	ENST00000656340	Novel gene	Decreased	5.10E-09
ENSG00000257261	ENST00000663959	Novel gene	Decreased	7.71E-10
ENSG00000232931	ENST00000660641	LINC00342	Decreased	5.75E-06
ENSG00000267432	ENST00000663269	DNAH17	Decreased	2.96E-12

Table 2: Top 5 increased and decreased DEmiRNAs.

miRNA	Status	logFC	*P* value
hsa-miR-6773-3p	Increased	3.61676331	0.002245373
hsa-miR-1250-3p	Increased	3.379810682	0.002053361
hsa-miR-6848-5p	Increased	2.780991902	0.00707793
hsa-miR-4506	Increased	2.226485819	8.45E-06
hsa-miR-7109-3p	Increased	2.184563759	0.034727373
hsa-miR-548a-3p	Decreased	−1.378214532	0.040108511
hsa-miR-4449	Decreased	−1.398551955	0.037313819
hsa-miR-4485-5p	Decreased	−1.50328227	0.01272798
hsa-miR-3182	Decreased	−1.644656839	1.41E-06
hsa-miR-215-5p	Decreased	−1.987458083	0.008964197

Table 3: Top 5 increased and decreased DEmRNAs.

Gene ID	Transcript	Gene name	Status	*P* value
ENSG00000129657	ENST00000430767	SEC14L1	Increased	6.56E-20
ENSG00000144580	ENST00000542068	CNOT9	Increased	1.13E-11
ENSG00000161016	ENST00000533397	RPL8	Increased	3.45E-09
ENSG00000149782	ENST00000325234	PLCB3	Increased	7.20E-30
ENSG00000145425	ENST00000512690	RPS3A	Increased	1.55E-24
ENSG00000084774	ENST00000403525	CAD	Decreased	1.34E-33
ENSG00000167881	ENST00000539137	SRP68	Decreased	7.75E-12
ENSG00000124532	ENST00000274747	MRS2	Decreased	2.38E-19
ENSG00000197713	ENST00000354506	RPE	Decreased	1.61E-11
ENSG00000254093	ENST00000519088	PINX1	Decreased	2.39E-18

component (CC), biological process (BP), and molecular function (MF). The Kyoto Encyclopedia of Gene and Genome (KEGG) is a predictive calculation tool on the basis of relevant knowledge. Given a complete set of genes on a chromosome, it can anticipate the relevance of protein interaction networks in a variety of biological functions. Herein, the *R* package (v 3.5.1) and clusterProfiler were applied for this analysis.

2.5. Protein-Protein-Interaction (PPI) Network on the DElncRNA, DEmiRNA, and DEmRNA. Then, the Search Tool for the Retrieval of Interacting Genes (STRING v 11.5, https://cn.string-db.org/) tool was adopted to map PPI networks for all DElncRNA, DEmiRNA, and DEmRNA with a composite interaction score ≥0.4. Cytoscape was adopted to visualize the PPI networks. The connectivity among DElncRNA ($n = 10$), DEmiRNA ($n = 3$), and DEmRNA ($n = 53$) with high degrees was demonstrated by an independent PPI network.

2.6. The LASSO Analysis and Prognostic Signature Model Construction on the above 53 DEmRNAs. After the screening of the top 53 DEmRNAs from the sequencing data of β-elemene-treated CRC cells, we performed the least absolute shrinkage and selection operator (LASSO) regression model by the "glmnet" package of the *R* language. The relationship between the partial likelihood deviation and log (lambda, λ) was plotted, and the important parameters of the signature model were obtained. Moreover, we downloaded clinical samples of CRC from The Cancer and Genome Atlas (TCGA, https://tcga-data.nci.nih.gov/tcga) dataset and analyzed the prognostic values of mRNAs in clinical. First, CRC samples were classified into high-risk ($n = 309$) and low-risk ($n = 310$) groups in the risk score analysis, and the

Figure 2: The GO and KEGG enrichment analyses on DElncRNAs, DEmiRNAs, and DEmRNAs. (a) The GO analysis of lncRNAs. (b) The KEGG pathway enrichment analysis of lncRNAs. (c) The GO analysis of miRNAs. (d) The KEGG pathway enrichment analysis of miRNAs. (e) The GO analysis of mRNAs. (f) The KEGG pathway enrichment analysis of mRNAs.

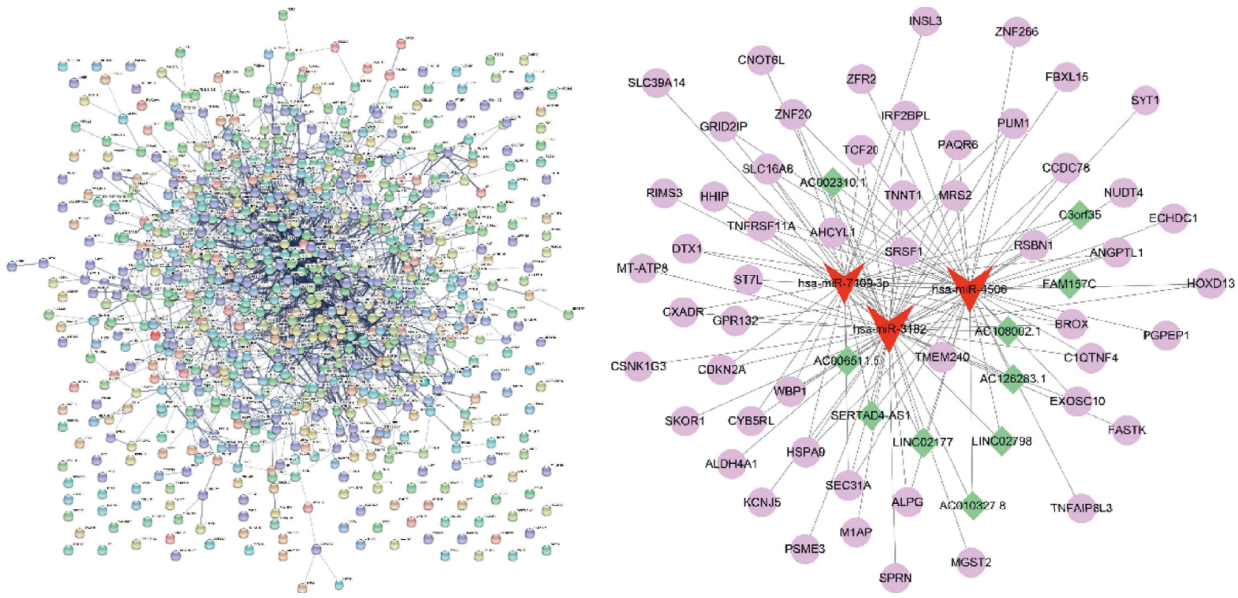

(a) (b)

Figure 3: The lncRNA-miRNA-mRNA coexpression network analysis. (a) The PPI network of the DERmNAs. (b) The lncRNA-miRNA-mRNA network of RNAs with top degrees in each category.

survival status of CRC samples corresponding to 15 different mRNAs was displayed. Next, the overall survival (OS) probability between two groups was compared by the Kaplan–Meier (KM, https://kmplot.com/analysis/) survival curve. Finally, the receiver operating characteristic (ROC) curve was used to compare the area under the curve (AUC) values of 1-, 3-, and 5-year survival rates of CRC, and the HR with 95% CI was calculated.

2.7. The Establishment of Prognostic Nomogram in CRC. To further verify the key mRNAs on the prognosis of CRC patients, the "forestplot" package was used to draw forest plots to display the results of univariate and multivariate Cox regression analyses on the above 15 mRNAs, and the corresponding P value and hazard ratio (HR) with 95% CI were calculated. Then, 7 mRNAs related to CRC prognosis were identified. Then, the corresponding nomogram was constructed by the "rms" package to predict the 1-, 3-, and 5-year survival rates with 7 prognostic mRNAs for CRC patients. The closer the dots are to the calibration curve, the higher the accuracy of this nomogram.

2.8. The Expression Verification and KM Analysis on the 7 Prognostic mRNAs. Based on the above findings, we detected their expressions in CRC tumor ($n = 620$) and normal ($n = 10$) samples in the TCGA database to identify the key mRNAs related to CRC. Then, the relations between the key mRNA expressions and OS and progression-free survival (PFS) curves were studied.

3. Results

3.1. DElncRNA, DEmiRNA, and DEmRNA from β-Elemene-Treated Samples. First, we analyzed the DElncRNA, DEmiRNA, and DEmRNA expression profiling data from β-elemene-treated samples. According to the RNA-seq analysis, 607 upregulated and 599 downregulated DElncRNAs were identified and displayed by volcano and heat maps (Figures 1(a) and 1(b)), and the top 5 upregulated and downregulated DElncRNAs are demonstrated in Table 1. As shown in Figures 1(c) and 1(d), we identified 12 downregulated and 24 upregulated DEmiRNAs, and the top 5 of each group are shown in Table 2. Besides, 3153 downregulated and 3248 upregulated DEmRNAs are displayed in Figures 1(e) and 1(f), and the top 5 DEmRNAs of them are also shown in Table 3.

3.2. The Results of GO Term and KEGG Pathway Enrichment Analyses. In GO analysis, DElncRNAs were enriched in positive regulation of muscle hyperplasia, regulation of B cell activation, lung growth (BP), and mRNA binding involved in posttranscriptional gene silencing (MF, Figure 2(a)). DEmiRNAs were enriched in negative regulation of transcription by RNA polymerase II, positive regulation of gene expression (BP), transcription regulator complex, chromatin, heteromeric SMAD protein complex (CC), DNA-binding transcription factor binding, and sequence-specific DNA binding (MF, Figure 2(c)). DEmRNAs were enriched in positive regulation of phospholipase C activity (BP), basolateral plasma membrane (CC), clathrin-coated vesicle membrane, and RNA polymerase III complex (MF, Figure 2(e)). In the KEGG pathway analysis, DElncRNAs were related to the CCL18 signaling pathway, ncRNAs involved in STAT3 signaling in hepatocellular carcinoma, lncRNA mediated mechanisms of therapeutic resistance (Figure 2(b)), DEmiRNAs were related to the integrated breast cancer pathway, the TGF-beta signaling pathway, senescence, and autophagy in cancer (Figure 2(d)), and

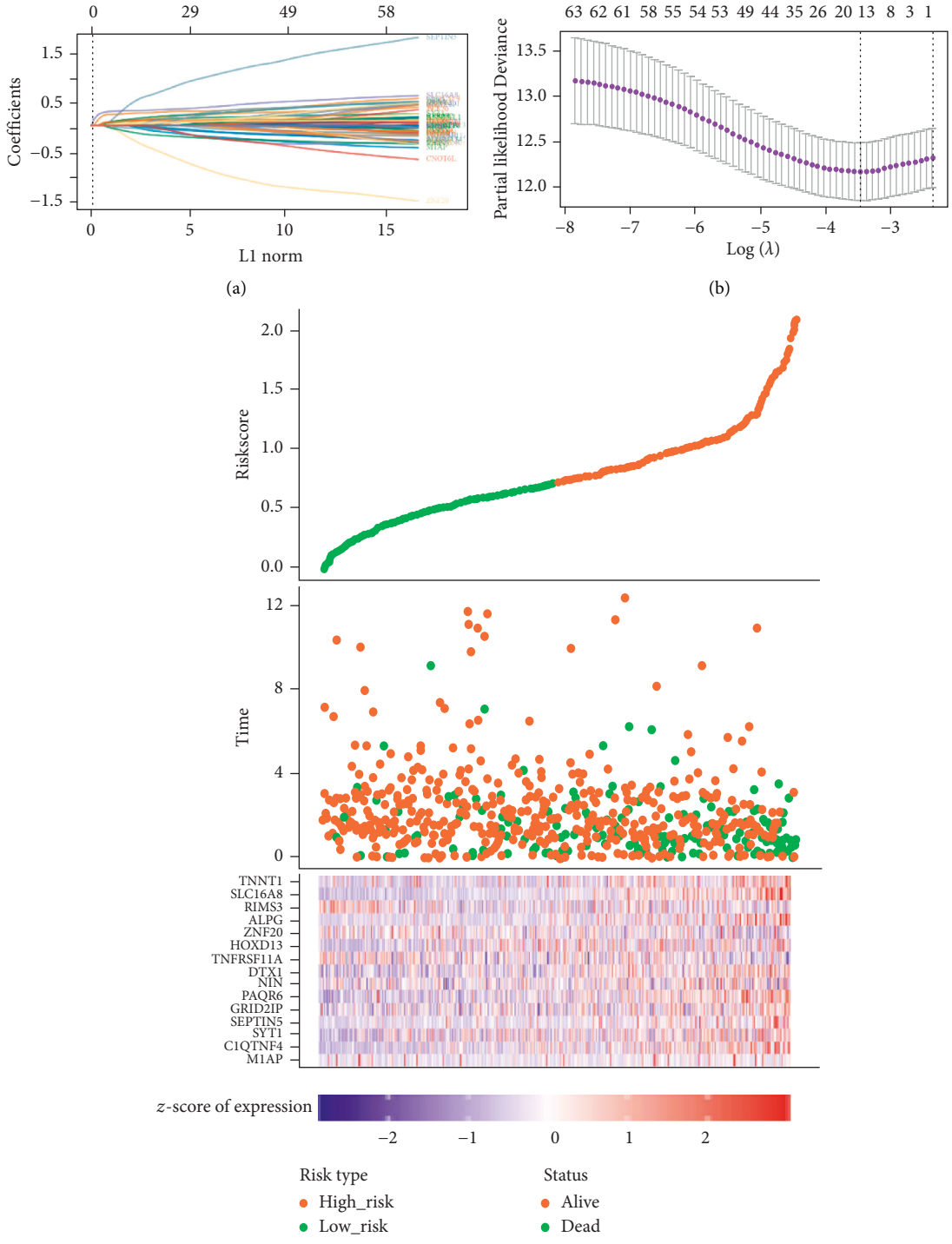

Figure 4: Continued.

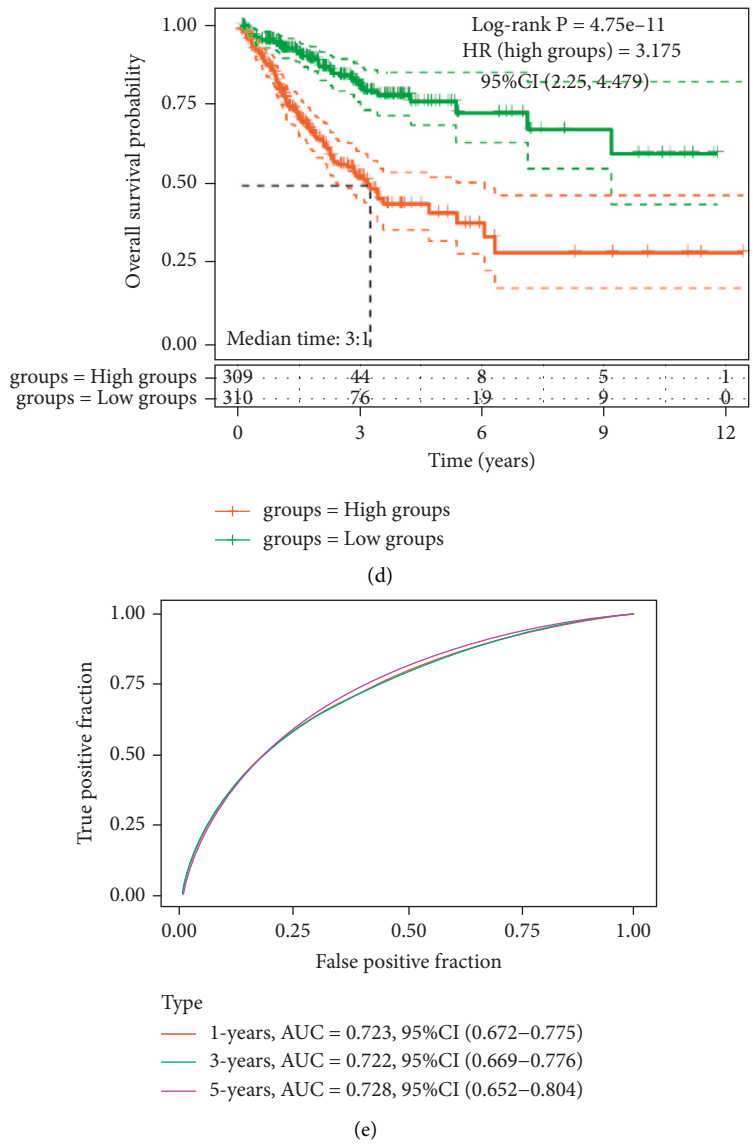

Figure 4: The LASSO analysis and prognostic signature model construction on the 53 mRNAs. (a)-(b) The LASSO regression mode analysis on the 53 mRNAs. (c) The risk score evaluation of CRC patients (top). The corresponding survival time of each patient (middle). The Z-score of expression of 15 candidate prognostic mRNAs (bottom). (d) Prognostic analysis of high-risk and low-risk groups. (e) The ROC curve analysis.

DEmRNAs were related to the ectoderm differentiation, the leptin signaling pathway, and so on (Figure 2(f)).

3.3. The lncRNA-miRNA-mRNA Coexpression Network Analysis. Next, we constructed a PPI network of the DERNAs with the Cytoscape tool (Figure 3(a)). According to the degrees in each group, DERNAs with high degrees (composite interaction score ≥0.4) in each group were selected for the construction of the lncRNA-miRNA-mRNA network, including 10 DElncRNAs, 3 DEmiRNAs, and 53 DEDmRNAs. As demonstrated in Figure 3(b), miR-7109-3p, miR-4506, and miR-3182 were closely related to ambient DElncRNAs and DEmRNAs, which indicated that miR-7109-3p, miR-4506, and miR-3182 had the potential to be clinical biomarkers or therapeutic targets in CRC.

Nodes represent genes, and edges represent interactions between genes. The green nodes represent the lncRNA, the red nodes represent the miRNA, and the purple nodes represent the mRNA.

3.4. The LASSO Analysis and Prognostic Signature Model Construction of the 53 DEmRNAs. The LASSO regression analysis was first performed on the above 53 DEmRNAs to determine the optimal parameter number of the signature model (Figures 4(a) and 4(b), each line represented a DEmRNA). Then, CRC samples in the TCGA database were divided into high- ($n = 309$) and low-risk groups ($n = 310$),

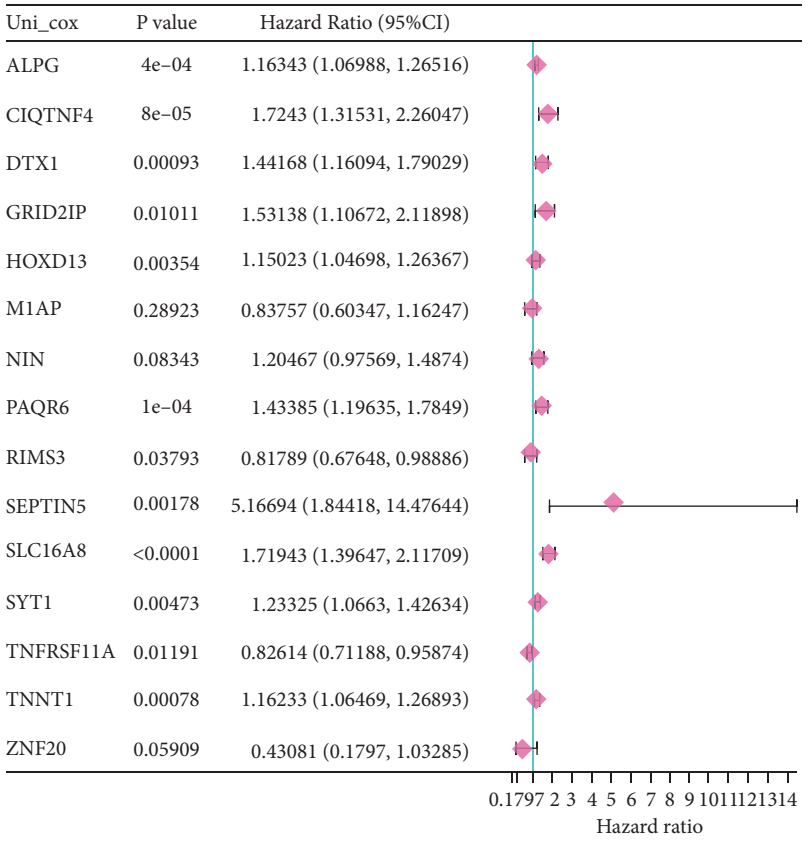

(a)

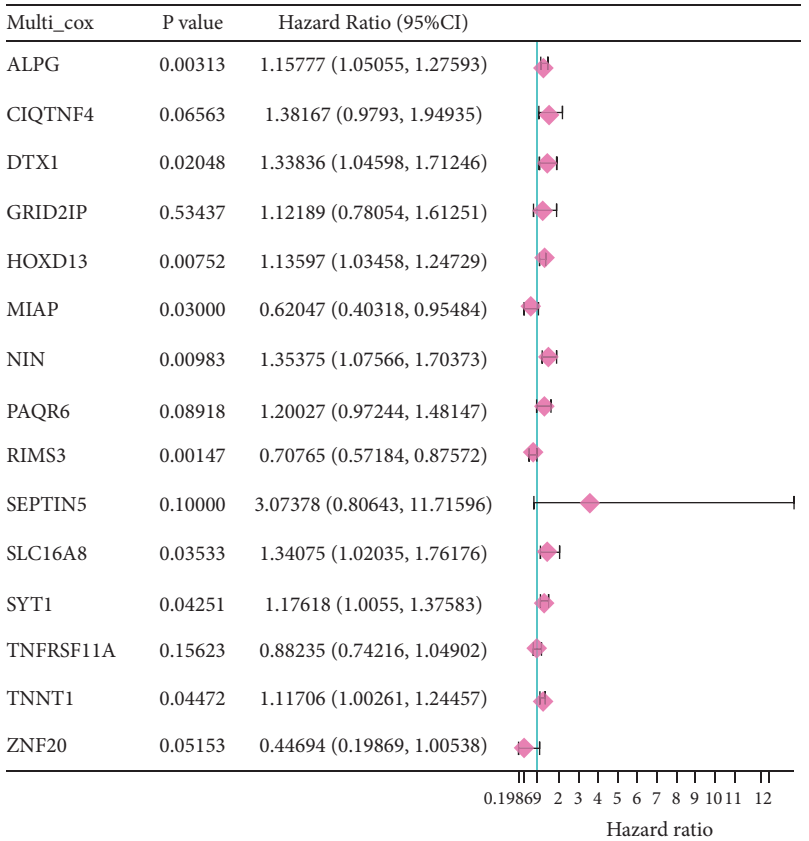

(b)

Figure 5: Continued.

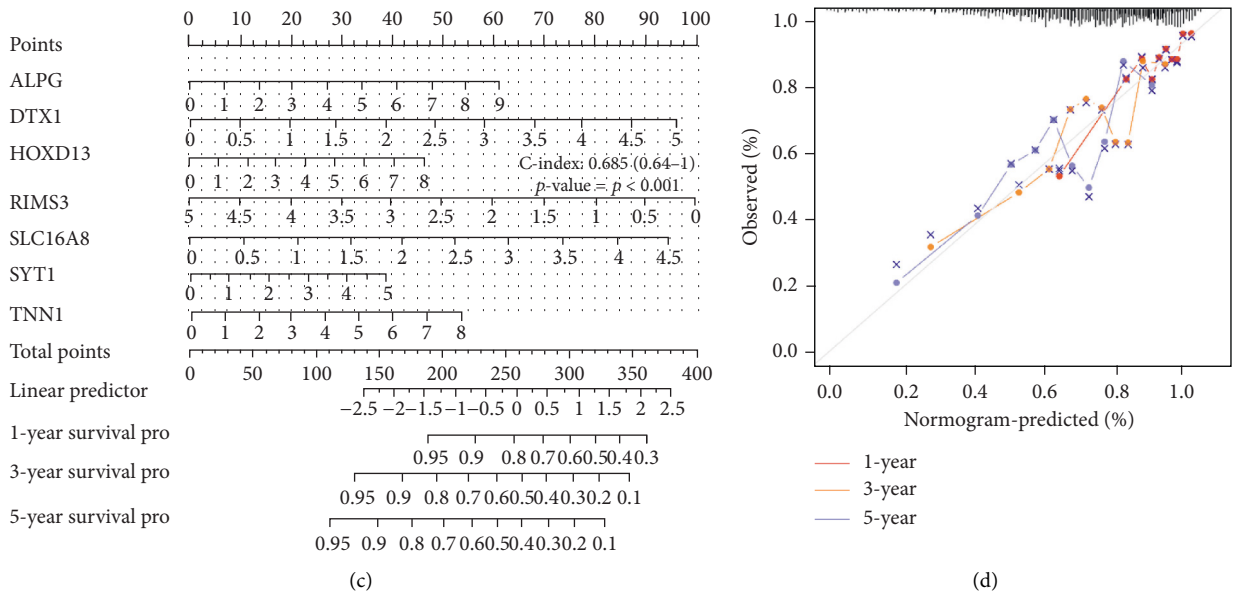

Figure 5: The prognostic nomogram with prognostic mRNAs. (a)-(b) Univariate and multivariate Cox regression analyses. (c) The prognostic nomogram with prognostic mRNAs. (d) The dotted line is the ideal calibration curve of the nomogram.

and it was found that the 15 mRNAs, M1AP, C1QTNF4, SYT1, SEPTIN5, GRID2IP, PAQR6, NIN, DTX1, TNFRSF11 A, HOXD13, ZNF20, ALPG, RIMS3, SLC16A8, and TNNT1, had the potential to be prognostic biomarkers in CRC (Figure 4(c)). In the KM survival curve, the median time of the two groups was 3.1 years, and the OS probability of the high-risk group was poor, and its HR was 3.175 (>1), indicating that the model was a risk model (Figure 4(d)). In addition, the AUC values in the ROC curve were all greater than 0.7, suggesting a good prognostic prediction ability of the model (Figure 4(e)).

3.5. The Identification of mRNAs with Prognostic Value in CRC. To investigate the mRNAs with prognostic values in CRC, we performed univariate and multivariate Cox regressions on the above 15 DEmRNAs. Under the premise of $P < 0.05$, it was found that ALPG, DTX1, HOXD13, RIMS3, SLC16A8, SYT1, and TNNT1 had a close relationship with the prognosis of CRC patients (Figures 5(a) and 5(b)). Subsequently, a nomogram on these genes was designed to predict the 1-, 3-, and 5-year survival rates of CRC patients (Figure 5(c)). As shown in Figure 5(d), the different dots were relatively close to the calibration curve, indicating that the prognostic model had good predictive ability.

3.6. RIMS3 and SLC16A8 Were the Key mRNAs Related to CRC in β-Elemene Treatment. To further explore the exact mRNAs related to CRC in β-elemene treatment, we detected the expressions of the 7 prognostic mRNAs in CRC tumor and normal samples. After detection, it was found that RIMS3 was significantly increased in normal samples, while SLC16A8 was substantially upregulated in tumor samples (Figures 6(a) and 6(d)), which indicated that RIMS3 was a suppressor gene while SLC16A8 was an oncogene in CRC. In the OS and PFS analyses on them, low expression of RIMS3 represented a poor survival rate, while low expression of SLC16A8 represented a relatively good survival rate (Figures 6(b), 6(c), 6(e), 6(f)).

4. Discussion

In recent years, the lncRNA-miRNA-mRNA network has been applied in the mechanism study of various diseases. For example, Li et al. found a novel lncRNA-miRNA-mRNA signature that predicted recurrence and disease-free survival in cervical cancer [19]. Cao et al. found through miR-206, lncRNA-RMRP increased bladder cancer development [20]. Besides, some researchers demonstrated lncRNA-CDC6 might act as a ceRNA to facilitate breast cancer development by sponging miRNA-215 [21]. In this study, we also tried to investigate the exact mechanism in β-elemene inhibiting CRC progression from the aspect of the lncRNA-miRNA-mRNA network.

Through deep sequencing, high-throughput screening, and microarray technology, many dysregulated miRNAs were found in cancer cells. Due to the tissue specificity of miRNA regulation, miRNAs have much potential to be biomarkers in cancer diagnosis, treatment, and prognosis [22]. In this study, we identified 1026 DElncRNAs, 6401 DEmRNAs, and 36 DEmiRNAs in β-elemene-treated HCT116 cells using RNA sequencing. Then, these DERNAs were analyzed by functional analyses and PPI networks. Enrichment analysis showed that DElncRNAs were associated with the CCL18 signaling pathway. Ruixue Yuan et al. showed that high CCL18 levels can be an independent biomarker for predicting better survival in CRC patients [23]. The DEmiRNAs were related to the TGF-beta signaling

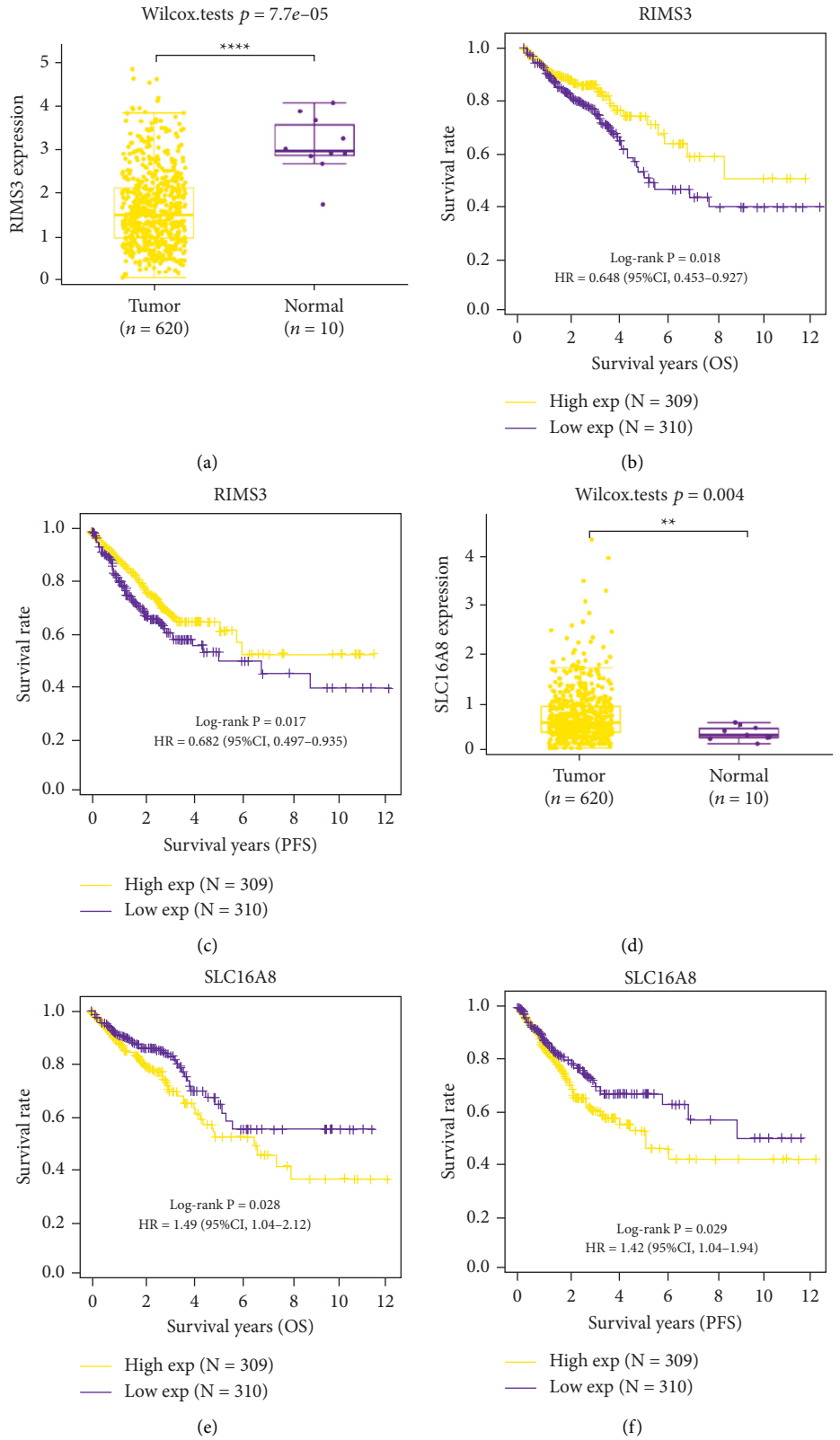

FIGURE 6: RIMS3 and SLC16A8 were the key mRNAs related to CRC in β-elemene treatment. (a) RIMS3 significantly downregulated in CRC samples. (b)-(c) The Kaplan–Meier survival curve showing that lower expression levels of RIMS3 were significantly associated with shorter OS and PFS in CRC. (d) SLC16A8 upregulated in tumor samples. (e)-(f) The Kaplan–Meier survival curve showing that higher expression levels of RIMS3 were significantly associated with shorter OS and PFS in CRC. $^{**}P < 0.01$, $^{****}P < 0.0001$.

pathway. TGF-beta signaling is one of the important cellular pathways that plays a key role in tissue maintenance. Nan et al. mentioned that LINC00941 plays an important role in metastatic CRC by activating the TGF-β/SMAD2/3 axis [24]. DEmRNAs are related to the leptin signaling pathway. Leptin is an activator of cell proliferation, an antiapoptotic molecule, and an inducer of cancer stem cells in many cell types. Studies have shown that the stringent binding affinity of leptin/Ob-R and the overexpression of leptin/Ob-R and its targets in cancer cells make it a unique drug target for the prevention and treatment of CRC, especially in obese colorectal patients [25]. In the PPI network, we selected the top RNAs in each group and observed their mutual relations, including miR-7109-3p, miR-4506, and miR-3182. At present, there are few reports on miR-7109-3p. One study highlights LINC00973-miR-7109-Siglec-15 function in the immune evasion of clear-cell renal cell carcinoma [26]. Nagy discovered miR-4506 was differentially expressed in adenoma compared to normal both in CRC tissue and plasma samples [27]. Moreover, it was found that the biological functions and potential mechanisms of miR-3182 were altered after Ganoderic acid treatment in CRC [28]. The 3 miRNAs all have the potential to be clinical biomarkers in CRC.

Besides, we focused on the mRNA associated with β-elemene and CRC. Through LASSO, risk score evaluation, and Cox analyses, 7 prognostic mRNAs, ALPG, DTX1, HOXD13, RIMS3, SLC16A8, SYT1, and TNNT1, were identified and applied to design the predictive nomogram for CRC prognosis, and the nomogram was proved to have a good prediction ability. In the previous research, few studies were conducted on these genes. In a study on TNNT1, researchers demonstrated that TNNT1, a target of miR-873, is related to CRC prognosis [29]. Herein, our findings show that the 7 mRNAs could be the prognostic biomarkers for CRC patients.

Furthermore, two key mRNAs related to CRC were identified by expression and KM analysis, namely, RIMS3 and SLC16A8. According to the public database, RIMS3 was a suppressor gene in CRC, while SLC16A8 was an oncogene in CRC. Regulating synaptic membrane exocytosis 3 (RIMS3) is supposed to enable transmembrane transporter binding activity and participate in the calcium ion-regulated exocytosis of neurotransmitters. Currently, it is suggested that RIMS3 is a gene related to autism. Functional investigations on RIMS3 variations like p.E177 A deepen our understanding of synaptic proteins' function in autism pathogenesis [30]. Additionally, solute carrier family 16 member 8 (SLC16A8), alias MCT3 and REMP, belongs to a family of proton-coupled monocarboxylate transporters regulating lactate transport across cell membranes [31]. The study of Klipfel L demonstrates the loss of transport function of the hypomorphic allele in the SLC16A8 gene and offers a methodological framework for the investigation of other SLC16A8 alleles linked to age-related macular degeneration [32]. Currently, there are no reports about these two genes in CRC development. Based on our study, we conclude that RIMS3 and SLC16A8 are the key mRNAs involved in the β-elemene treatment in CRC progression, which certainly reveals the inhibitory mechanism of β-elemene in CRC. The study still has limitations. First, the expression profiles given by differential expression need to be validated with clinical samples. Second, further experimental studies are required to confirm the function of the lncRNA-miRNA-mRNA network in the inhibition of CRC progression by β-elemene.

To sum up, this study reveals the lncRNA-miRNA-mRNA network in the inhibitory function of β-elemene in CRC. These identified differentially expressed mRNAs (RIMS3 and SLC16A8) and miRNAs (miR-7109-3p, miR-4506, and miR-3182) all could be promising clinical biomarkers or targets in CRC diagnosis, treatment, and prognosis.

Data Availability

The datasets used to support the findings of this study are available from the corresponding author upon request.

Conflicts of Interest

The authors declare that they have no conflicts of interest.

Acknowledgments

This study was funded by the Natural Science Foundation of Anhui Province (2008085QH388) and Clinical Research Project of the Anhui University of Chinese Medicine (2021efylc02).

References

[1] N. Akimoto, T. Ugai, R. Zhong et al., "Rising incidence of early-onset colorectal cancer - a call to action," *Nature Reviews Clinical Oncology*, vol. 18, no. 4, pp. 230–243, 2021.

[2] N. Keum and E. Giovannucci, "Global burden of colorectal cancer: emerging trends, risk factors and prevention strategies," *Nature Reviews Gastroenterology & Hepatology*, vol. 16, no. 12, pp. 713–732, 2019.

[3] T. Sawicki, M. Ruszkowska, A. Danielewicz, E. Niedzwiedzka, T. Arlukowicz, and K. E. Przybylowicz, "A review of colorectal cancer in terms of epidemiology, risk factors, development, symptoms and diagnosis," *Cancers*, vol. 13, no. 9, p. 2025, 2021.

[4] S. K. P. John, S. George, J. N. Primrose, and J. B. J. Fozard, "Symptoms and signs in patients with colorectal cancer," *Colorectal Disease*, vol. 13, no. 1, pp. 17–25, 2011.

[5] F. Baidoun, K. Elshiwy, Y. Elkeraie et al., "Colorectal cancer epidemiology: recent trends and impact on outcomes," *Current Drug Targets*, vol. 22, no. 9, pp. 998–1009, 2021.

[6] S. Ye, L. Yang, X. Zhao, W. Song, W. Wang, and S. Zheng, "Bioinformatics method to predict two regulation mechanism: TF–miRNA–mRNA and lncRNA–miRNA–mRNA in pancreatic cancer," *Cell Biochemistry and Biophysics*, vol. 70, no. 3, pp. 1849–1858, 2014.

[7] Y. Zhang, Y. Li, Q. Wang et al., "Identification of an lncRNA-miRNA-mRNA interaction mechanism in breast cancer based on bioinformatic analysis," *Molecular Medicine Reports*, vol. 16, no. 4, pp. 5113–5120, 2017.

[8] R.-S. Zhou, E. X. Zhang, Q. F. Sun et al., "Integrated analysis of lncRNA-miRNA-mRNA ceRNA network in squamous cell carcinoma of tongue," *BMC Cancer*, vol. 19, no. 1, p. 779, 2019.

[9] A. Link and J. Kupcinskas, "MicroRNAs as non-invasive diagnostic biomarkers for gastric cancer: current insights and future perspectives," *World Journal of Gastroenterology*, vol. 24, no. 30, pp. 3313–3329, 2018.

[10] P. M. Pereira, J. P. Marques, A. R. Soares, L. Carreto, and M. A. S. Santos, "MicroRNA expression variability in human cervical tissues," *PloS One*, vol. 5, no. 7, Article ID e11780, 2010.

[11] A. Fonseca, S. V. Ramalhete, A. Mestre et al., "Identification of colorectal cancer associated biomarkers: an integrated analysis of miRNA expression," *Aging (Albany NY)*, vol. 13, no. 18, pp. 21991–22029, 2021.

[12] Y. Feng, C. Li, S. Liu et al., "*β*-Elemene restrains PTEN mRNA degradation to restrain the growth of lung cancer cells via METTL3-mediated N(6) methyladenosine modification," *Journal of Oncology*, vol. 2022, pp. 1–11, 2022.

[13] Y. Pan, W. Wang, S. Huang et al., "Beta-elemene inhibits breast cancer metastasis through blocking pyruvate kinase M2 dimerization and nuclear translocation," *Journal of Cellular and Molecular Medicine*, vol. 23, no. 10, pp. 6846–6858, 2019.

[14] P. Chen, X. Li, R. Zhang et al., "Combinative treatment of *β*-elemene and cetuximab is sensitive to KRAS mutant colorectal cancer cells by inducing ferroptosis and inhibiting epithelial-mesenchymal transformation," *Theranostics*, vol. 10, no. 11, pp. 5107–5119, 2020.

[15] X. Zhang, Y. Chen, J. Yao et al., "*β*-elemene combined with temozolomide in treatment of brain glioma," *Biochemistry and Biophysics Reports*, vol. 28, Article ID 101144, 2021.

[16] S. Zhang and W. Guo, "*β*-Elemene enhances the sensitivity of osteosarcoma cells to doxorubicin via downregulation of peroxiredoxin-1," *OncoTargets and Therapy*, vol. 14, pp. 3599–3609, 2021.

[17] W. Zhan, H. Li, Y. Guo, G. Du, Y. Wu, and D. Zhang, "Construction of biocompatible dual-drug loaded complicated nanoparticles for in vivo improvement of synergistic chemotherapy in esophageal cancer," *Frontiers in Oncology*, vol. 10, p. 622, 2020.

[18] G. Y. Wang, *The Study on the Effect and Mechanism of β-elemene in Colorectal Cancer*, Anhui Medical University, Hefei, China, 2018.

[19] M. Li, X. Tian, H. Guo et al., "A novel lncRNA-mRNA-miRNA signature predicts recurrence and disease-free survival in cervical cancer," *Brazilian Journal of Medical and Biological Research*, vol. 54, no. 11, Article ID e11592, 2021.

[20] H. L. Cao, Z. J. Liu, P. L. Huang, Y. L. Yue, and J. N. Xi, "lncRNA-RMRP promotes proliferation, migration and invasion of bladder cancer via miR-206," *European Review for Medical and Pharmacological Sciences*, vol. 23, no. 3, pp. 1012–1021, 2019.

[21] X. Kong, Y. Duan, Y. Sang et al., "LncRNA–CDC6 promotes breast cancer progression and function as ceRNA to target CDC6 by sponging microRNA-215," *Journal of Cellular Physiology*, vol. 234, no. 6, pp. 9105–9117, 2019.

[22] Y. Xu, R. Geng, F. Yuan, Q. Sun, B. Liu, and Q. Chen, "Identification of differentially expressed key genes between glioblastoma and low-grade glioma by bioinformatics analysis," *PeerJ*, vol. 7, Article ID e6560, 2019.

[23] R. Yuan, Y. Chen, X. He et al., "CCL18 as an independent favorable prognostic biomarker in patients with colorectal cancer," *Journal of Surgical Research*, vol. 183, no. 1, pp. 163–169, 2013.

[24] N. Wu, M. Jiang, H. Liu et al., "LINC00941 promotes CRC metastasis through preventing SMAD4 protein degradation and activating the TGF-*β*/SMAD2/3 signaling pathway," *Cell Death & Differentiation*, vol. 28, no. 1, pp. 219–232, 2021.

[25] W. Zhou, Y. Tian, H. Gong, S. Guo, and C. Luo, "Oncogenic role and therapeutic target of leptin signaling in colorectal cancer," *Expert Opinion on Therapeutic Targets*, vol. 18, no. 8, pp. 961–971, 2014.

[26] D. S. Karpov, P. V. Spirin, A. O. Zheltukhin et al., "LINC00973 induces proliferation arrest of drug-treated cancer cells by preventing p21 degradation," *International Journal of Molecular Sciences*, vol. 21, no. 21, p. 8322, 2020.

[27] Z. B. Nagy, B. Wichmann, A. Kalmar et al., "Colorectal adenoma and carcinoma specific miRNA profiles in biopsy and their expression in plasma specimens," *Clinical Epigenetics*, vol. 9, no. 1, p. 22, 2017.

[28] N. Chen, G. Wan, and X. Zeng, "Integrated whole-transcriptome profiling and bioinformatics analysis of the polypharmacological effects of ganoderic acid me in colorectal cancer treatment," *Frontiers in Oncology*, vol. 12, Article ID 833375, 2022.

[29] Y. Chen, J. Wang, D. Wang et al., "TNNT1, negatively regulated by miR-873, promotes the progression of colorectal cancer," *The Journal of Gene Medicine*, vol. 22, no. 2, Article ID e3152, 2020.

[30] R. A. Kumar, J. Sudi, T. D. Babatz et al., "A de novo 1p34.2 microdeletion identifies the synaptic vesicle gene RIMS3 as a novel candidate for autism," *Journal of Medical Genetics*, vol. 47, no. 2, pp. 81–90, 2010.

[31] H. Yoon, L. A. Donoso, and N. J. Philp, "Cloning of the human monocarboxylate transporter MCT3 gene: localization to chromosome 22q12.3-q13.2," *Genomics*, vol. 60, no. 3, pp. 366–370, 1999.

[32] L. Klipfel, M. Cordonnier, L. Thiebault et al., "A splice variant in SLC16A8 gene leads to lactate transport deficit in human iPS cell-derived retinal pigment epithelial cells," *Cells*, vol. 10, no. 1, p. 179, 2021.

Hindawi
Genetics Research
Volume 2022, Article ID 9313559, 8 pages
https://doi.org/10.1155/2022/9313559

Research Article

ABIN1 Inhibits Inflammation through Necroptosis-Dependent Pathway in Ulcerative Colitis

Jing Bao, Bin Ye, and Yuhan Ren

Department of Gastroenterology, Shengzhou People's Hospital, Shaoxing, China

Correspondence should be addressed to Yuhan Ren; zihan_ren@126.com

Received 12 May 2022; Accepted 5 July 2022; Published 8 August 2022

Academic Editor: Jun Yang

Background. Ulcerative colitis (UC) is characterized by chronic, recurrent intestinal inflammation and intestinal epithelial injury including a wide range of epithelial cell death, ulcers, crypt abscesses, and the formation of fibrosis. The intestinal barrier dysfunction runs through the whole process of the occurrence and development of UC. A recent study revealed that an ubiquitin binding protein ABIN1 played a role in tissue homeostasis and autoimmunity diseases which involved in the anti-inflammatory response of intestinal epithelia cells. However, the roles of ABIN1 in ulcerative colitis pathogenesis remain unclear. *Methods*. The mRNA and protein expression level of ABIN1 and necroptosis-associated genes (RIPK1, RIPK3, and MLKL) were conducted to investigate the relationship between ABIN1 and necroptosis in clinical UC specimens. Subsequently, the dextran sodium sulfate (DSS)-induced mice colitis model was used to verify the ABIN1 function in vivo. Furthermore, we established ABIN1 gain and loss function assay in CACO-2 to confirm the mechanism in UC in vitro. *Results*. We found that ABIN1, RIPK1, RIPK3, and MLKL were upregulated in UC sample and DSS-induced colitis. Upon TNF-α stimulation in the intestinal epithelia cell line, overexpression of ABIN1 significantly inhibits necroptosis in the intestinal inflammation model along with the reduction expression of pro-inflammatory cytokines such as IL1B, IL6, IL8, and TNF-α. Blocking RIPK1 by Nec-1s *in vivo* and *in vitro* dramatically alleviated the colitis and cell death which shares the same phenotype with ABIN1 overexpression. *Conclusion*. Hence, the dysregulation of ABIN1 may relate to the uncontrolled necroptosis and inflammation in UC, and negatively regulate the occurrence and process of ulcerative colitis. ABIN1 activation may be considered a therapeutic strategy for UC.

1. Introduction

Inflammatory bowel disease (IBD) is mainly represented by Crohn's disease (CD) and ulcerative colitis (UC) [1]. Unlike Crohn's disease that could occur anywhere in total intestinal tract, UC primarily affects the colon and rectum, is characterized by chronic, recurrent intestinal inflammation and intestinal epithelial injury including a wide range of epithelial cell death, ulcers, crypt abscesses, and the formation of fibrosis. The etiology of UC is complex and diverse, which is related to monogenic/polygenic inheritance, microbial/environment, intestinal barrier, and intestinal immune system [2]. The intestinal barrier dysfunction runs through the whole process of the occurrence and development of UC [3]. And the intestinal barrier is mainly formed by the physical isolation of exogenous microorganisms and endogenous immune cells through the large amount of mucus secreted by intestinal cells and the tight intercellular junctions between intestinal epithelial cells [4]. Therefore, impaired intestinal mucosal barrier function may be an important factor in susceptibility to UC.

In the process of UC, it has been found that intestinal epithelial cells were involved in four kinds of death forms: apoptosis, pyroptosis, anoikis, and programmed necrosis (necroptosis) according to different cell subtypes [5]. Among them, necroptosis is most likely to cause inflammation, which is initially provoked by ligand biding to tumor necrosis factor receptors(TNFR) and then activates receptor interacting serine/threonine kinase 1(RIPK1) to recruit receptor interacting serine/threonine kinase 1(RIPK3) as downstream mediator and ultimately phosphorylate mixed lineage kinase domain-like(MLKL) protein results in

membrane rupture, cell swelling, release of damage-associated molecular patterns (DAMPs) and leads to the development to various inflammatory diseases [6, 7].

Previous study shows that upon stimulation of TNF-α, an important proinflammatory cytokine involved in regulating various inflammatory diseases, RIPK1 acts as a critical regulator of necroptosis [8]. Activated RIPK1 has been indicated to be crucial for several inflammatory diseases including amyotrophic lateral sclerosis [9], multiple sclerosis [10], and IBD [11]. However, the kinase activity of RIPK1 is mediated by the post-translation modification such as phosphorylation and ubiquitination. According to the research of Slawomir et al., upon TNF-α stimulation, ABIN1, a ubiquitin binding protein, can suppress necroptosis by recruiting A20 to TNFR1 signaling complex (TNF-RSC) which mediates the deubiquitination of RIPK1 [12–14]. Furthermore, several genetic mutations of ABIN1 which lead to lower expression of ABIN1 are also dramatically related to some inflammatory diseases [15, 16]. Meanwhile, the survival of ABIN1-deficient mice can be prolonged through RIPK3 knockout or inactivation of RIPK1 to block necroptosis [12]. However, the contribution of the ABIN1 in ulcerative colitis pathogenesis remains unclear. Such evidence prompts that ABIN1 plays a critical role in suppressing RIPK1-mediated necroptosis in ulcerative colitis.

In this study, we investigate the expression level of ABIN1 and necroptosis key mediators in ulcerative colitis samples and dextran sodium sulfate-induced colitis models in mice. We found that ABIN1, RIPK1, RIPK3, and MLKL were upregulated in UC samples and DSS-induced colitis. Upon TNF-α stimulation in the intestinal epithelia cell line, overexpression of ABIN1 significantly inhibits necroptosis in the intestinal inflammation model along with the reduction expression of proinflammatory cytokines such as IL1B, IL8, and TNF-α. Blocking RIPK1 by Nec-1s *in vivo* (DSS-induced colitis in mice) and *in vitro* (TNF-α induced inflammation in the IEC cell line) dramatically alleviated the colitis and cell death which shares the same phenotype with ABIN1 overexpression. Hence, we hypothesized that the dysregulation of ABIN1 related to the uncontrolled necroptosis and inflammation in UC, and negatively regulates the occurrence and process of ulcerative colitis.

2. Method and Material

2.1. Patients' Specimens and Animal Treatment. For this study, normal ($n = 10$) and UC ($n = 10$) colon mucosal biopsies were obtained from healthy control and UC patients at Shengzhou People's Hospital from May 2014 to June 2017. The fresh UC specimens and normal mucosal were placed in liquid nitrogen for storage. All patients in this project have signed the informed consent and the study was reviewed and approved by the Ethics Committees of the Shengzhou People's Hospital. 6 to 8 week-old male C57BL/6 mice (20–24 g) were purchased from Charles River animal centre (Shanghai, China) and maintained in SPF facility. For the model of ulcerative colitis, mice were randomly divided into 4 groups ($n = 6$), vehicle group, DSS group, siABIN1+DSS group, and N1 + DSS + Nec-1s group. As described previously, mice were fed with 3.5% DSS (MP Biomedicals) for a week while the control group was given the same volume of distill water, as for siABIN1 + DSS group, mice were injected an additional 20 nm of siABIN1 (RIBOBIO, Guangzhou) every other day through tail vein. Meanwhile, the siABIN1 + DSS + Nec-1s group were added to daily drinking water based on the siABIN1 + DSS group. Each mouse was weighed and monitored for the appearance of blood and loose stool from day 1 to day 7. After a week, all mice were sacrificed, and then DAI score and the histopathological scores of mice were assessed as described in the previous work [17].

2.2. Cell Culture and Treatment. Human intestinal epithelia cell CACO-2 and 293T cell line were obtain from the American Type Culture Collection (ATCC). They were maintained in RPMI/1640 or high-glucose DMEM medium (Hyclone) supplemented with 10% fetal bovine serum (Gibco). Cells were cultured in a humidified incubator with 5% CO2 at 37°C. CACO-2 cell were treated with TNF-α (Sigma) and Nec-1s as described previously [17, 18]. As for RNA interference, cells were transfected with si-control and si-ABIN1, respectively, after premixing with Lipofectamine 3000 and incubated for 72 h.

si-ABIN1#1 GGTGCACACACCCTCGTATTC; si-ABIN1#2 GGAGCCTTCATAGGGACAGCC.

2.3. Extraction of RNA and Quantitative RT-PCR. Patients' mucosal, DSS-induced colon tissue and CACO-2 cell were applied for total RNA extraction. Total RNA was reverse transcribed into cDNA by TOYOBO ReverTra Ace kit (TOYOBO). Subsequently, 0.5 ug cDNA was subjected by using the SYBR system (Takara) following the manufacturer's instructions in an CFX (Bio-Rad) real-time PCR machine. The mRNA expression level was calculated by the $2^{-\Delta\Delta Ct}$ method. The final values were normalized to the mRNA expression of β-ACTIN. The primers of β-ACTIN, ABIN1, RIPK1, MLKL, IL1B, IL8, TNF-α, and RIPK3 used for qRT-PCR are shown in Table 1.

2.4. Western Blot Analysis. Total proteins were extracted from patents' specimens, DSS-induced colon tissue, and cell lines by 1% NP40 lysis. Protein concentration was detected by Braford Kit (Beyotime). In performing Western blot, 20 mg protein were separated on different concentrations of SDS-PAGE gel and by following the standard protocol of WB. After ECL exposure, the protein expression level was calculated by gray value through ImageJ.

2.5. Statistical Analysis. The results are shown as the mean ± SD. Differences in mean values between two groups were analyzed by two-tailed Student's t test. P values less than 0.05 were considered statistically significant, and the statistical analysis was conducted in GraphPad Prism6.

3. Results

3.1. ABIN1 is Markedly Increased in the UC Samples. ABIN1 plays a role in tissue homeostasis and autoimmunity diseases which involved in the anti-inflammatory response

Table 1: The sequence of qRT-pcr primers.

qRT-PCR primer	Forward (5′–3′)	Reverse (5′–3′)
β-ACTIN	CACCATTGGCAATGAGCGGTTC	AGGTCTTTGCGGATGTCCACGT
RIPK1	TATCCCAGTGCCTGAGACCAAC	GTAGGCTCCAATCTGAATGCCAG
RIPK3	GCTACGATGTGGCGGTCAAGAT	TTGGTCCCAGTTCACCTTCTCG
MLKL	TCACACTTGGCAAGCGCATGGT	GTAGCCTTGAGTTACCAGGAAGT
IL1B	CCACAGACCTTCCAGGAGAATG	GTGCAGTTCAGTGATCGTACAGG
IL6	AGACAGCCACTCACCTCTTCAG	TTCTGCCAGTGCCTCTTTGCTG
IL8	GAGAGTGATTGAGAGTGGACC	CACAACCCTCTGCACCCAGTTT
TNF-α	CTCTTCTGCCTGCTGCACTTTG	ATGGGCTACAGGCTTGTCACTC

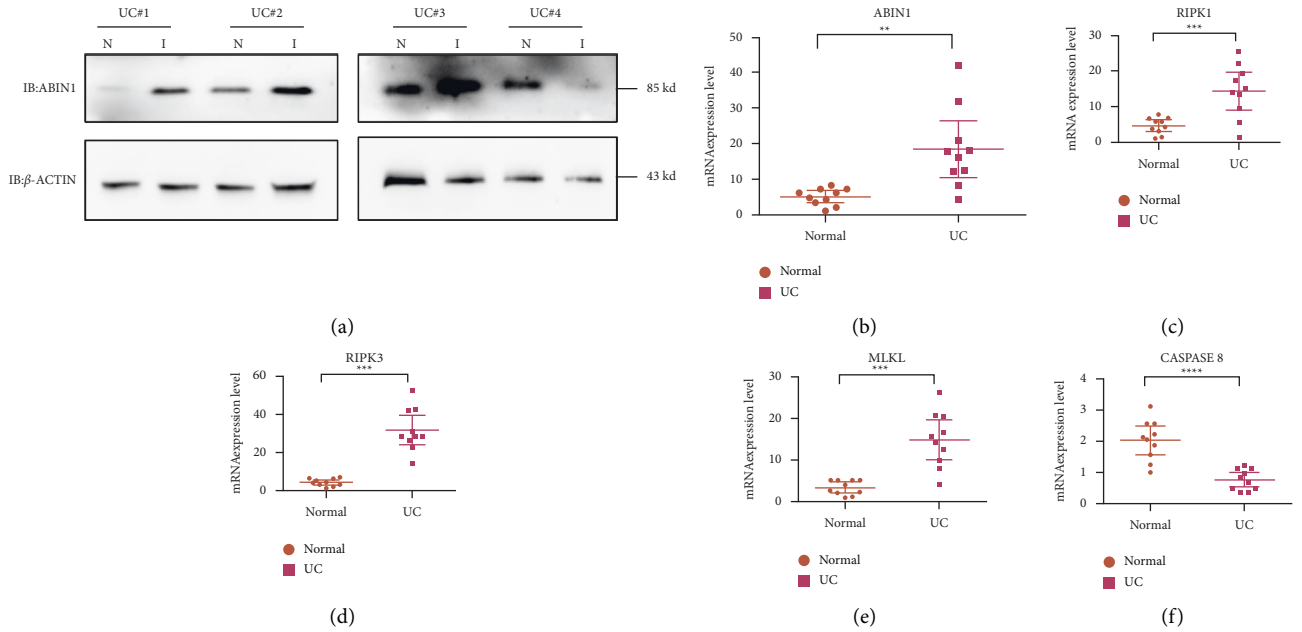

Figure 1: ABIN1 is markedly increased in the UC samples. (a) ABIN1 protein expression level was assessed in 4 pairs of UC patients; (b)–(f) the mRNA expression level of ABIN1, RIPK1, RIPK3, MLKL, and CASPASE8 were detected in ten pairs of UC patients' mucosal and adjacent normal tissues. Two-tailed student's t-test was performed to assess statistical significance $^{**}P < 0.01$, $^{***}P < 0.001$.

of intestinal epithelia cells. So, we investigate the mRNA and protein expression level of ABIN1 in 10 pairs of UC samples. The results show that ABIN1 mRNA expression level was significantly upregulated with value $P < 0.017$ (Figure 1(a)) and 3 in 3 pairs of ABIN1 protein expression level in inflamed colon were significantly increased as well (Figure 1(b)).

As discussed in the previous study, ABIN1 coordinates with A20 and regulates the ubiquitination of core necroptosis mediator RIPK1. We investigate the necroptosis level by determining mRNA expression level of CASPASE8, RIPK1, RIPK3, and MLKL in UC specimens compared with these levels in the adjacent normal tissues. The results show a remarkable increase in RIPK1 ($P < 0.009$), RIPK3 ($P < 0.001$), and MLKL ($P < 0.001$) in mRNA expression level (Figures 1(c)–1(e)), and CASPASE8 was significantly downregulated in UC (Figure 1(f)) indicating ABIN1 involvement causing increased necroptosis level *in vivo*.

3.2. ABIN1 Inhibits Necroptosis and the Expression of Proinflammatory Cytokines in IEC. To unveil the function of ABIN1 in mediating necroptosis and intestinal inflammation, we constructed an ABIN1 ectopic expression stable in the intestinal epithelial cell line. As shown in (Figures 2(a) and 2(b)), we successfully established ANBIN1 overexpression in the CACO-2 cell line. Upon TNF-α stimulation in CACO-2 cells, overexpression of ABIN1 remarkably reduced the mRNA expression level of proinflammatory cytokines including TNF-α (Figure 2(c)), IL-6 (Figure 2(c)), IL1B (Figure 2(c)), and IL8 (Figure 2(c)). Besides the protein expression of necroptosis core components RIPK1, RIPK3, and MLKL were decreased as well (Figure 2(b)). To further verify the function of ABIN1 in IEC, we used siRNA of ABIN1 to block the expression in CACO-2 cells (Figure 3(a)). The results uncovered that knockdown ABIN1 leads to the accentuation of necroptosis through increasing the expression of RIPK1, RIPK3, and MLKL (Figure 3(b)). Meanwhile, the expression of TNF-α, IL-6, IL1B, and IL8 were upregulated under TNF-α stimulation *in vitro* (Figure 3(c)).

3.3. Nec-1s Mitigates the Necroptosis-Associated Protein Expression and Intestinal Damage in ABIN1 Deficiency DSS-Induced Mice. Nec-1s, a RIPK1 inhibitor which plays a

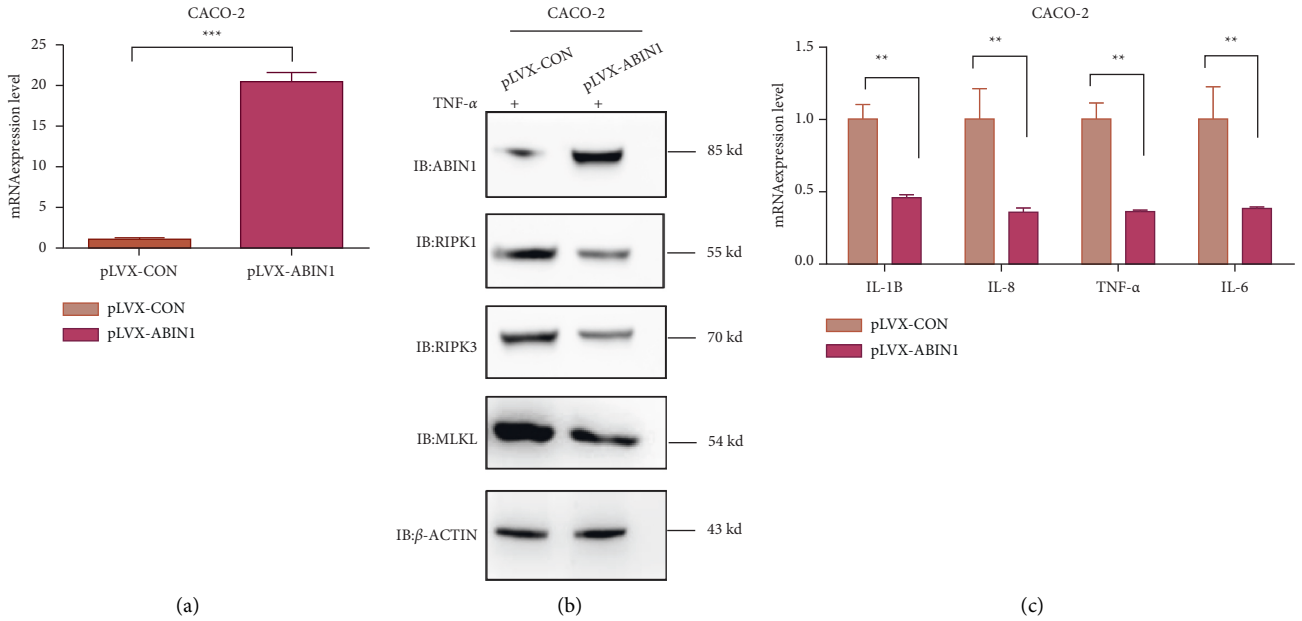

Figure 2: ABIN1 overexpression in IEC inhibits necroptosis and the expression of proinflammatory cytokines in IEC: (a) mRNA expression level overexpression verification in CACO-2 cells; (b) Necroptosis-associated proteins detection in CACO-2 ABIN1 overexpression stable upon TNF-α stimulation; and (c) mRNA expression level of proinflammatory cytokines in ABIN1 overexpression CACO-2 cells. Two-tailed Student's t-test was performed to assess statistical significance. $^{**}P < 0.01$, $^{***}P < 0.001$.

potent role in anti-inflammatory, was subjected to investigate the relationship between ABIN1 and RIPK1 in the DSS-induced colitis model. Mice were treated with 2.5% DSS for 7 days to bring symptoms of UC, such as loose stool, diarrhea, and weight loss, and then, we maintained DSS-induced mice with a daily treatment of si-ABIN1 or si-ABIN1 combined with Nec-1s treatment. We detected the mRNA expression level of ABIN1 in the DSS-induced colitis model (Figure 4(a)). The daily change of body weight and DAI was represented in Figure 4(a). The body weight of DSS + si-ABIN1 treatment group was significantly reduced from day 6 to day 7 compared to the DSS-treated group (DSS vs DSS + si-ABIN1, 18.52 ± 0.42 vs. 15 ± 0.32, $P < 0.05$); however, the body weight of the combination of DSS, si-ABIN1, and Nec-1s treatment group was conversely recovered when compared to DSS + si-ABIN1 group (DSS + si-ABIN1vs DSS + ABIN1 + Nec-1s, 15.25 ± 0.36 vs. 20.29 ± 0.22, $P < 0.01$). As for DAI comparison (Figure 4(b)), the similar result had shown combining Nec-1s mitigates the DAI, which is aggravated by ABIN1 deficiency. (DSS + si-ABIN1 vs. DSS + ABIN1+Nec-1s, 4.6 ± 0.38 vs 3.28 ± 0.21., $P < 0.01$).

Next, HE staining of the colon was conducted to evaluate the histological changes. DSS treatment caused muscle thickening, crypt damage, and lymphocyte infiltration and si-ABIN1 aggravates the intestinal injuries; however, adding the Nec-1s, inhibitor of RIPK1, greatly reduced these symptoms (Figure 4(c)). To further testify the relationship of ABIN1- and RIPK1-related necroptosis *in vitro*, we exposed colonic epithelial cell (Caco2) to Nec-1s upon TNF-α stimulation with or without the ablation of ABIN1. The results showed that Nec-1s could restore the increase of proinflammatory cytokines induced by ABIN1 ablation. And the upregulation of necroptosis-associated protein by ABIN1 ablation is also inhibited by the treatment of Nec-1s (Figure 4(d)).

4. Discussion

Intestinal barrier injury is the main symptom of UC which is induced by the abnormal cell death and proliferation in IEC. Cell death can be divided into four forms such as apoptosis, pyroptosis, anoikis, and necroptosis [5]. Unlike other forms of death forms, necroptosis was mainly induced in the TNF-α-mediating pathway which led to imbalance in cell death and proliferation of IEC. In necroptosis, RIPK1 is the core mediator which was initially discovered by screening for proteins that bind to the death receptor Fas [19]. Subsequently, research studies confirmed that RIPK1 was involved in TNF-α signaling as a skeleton protein to activate the NF-κB pathway [20]. Then, in 2000, Holler et al. [8] found that RIPK1 kinases were related in cell non-caspase-dependent necrosis. In 2005, Degterev et al. [21] formally named RIPK1-dependent cell necrosis as programmed necrosis. Thus, RIPK1 is a dual-functional protein: one function depends on its protein skeleton and the other on its kinase activity. The functional diversity of RIPK1 is also reflected in transgenic mice. Mice with RIPK1 protein deletion can only survive for 3 days [22], but mice with RIPK1 kinase activity deletion can survive normally [23]. In addition, it has also been reported in recent years that RIPK1 is related to human inflammatory diseases [24]. The deletion mutation of RIPK1 gene can lead to severe immune deficiency and other diseases, while another missense mutation of RIPK1 gene can lead to inflammatory diseases [25]. Knockout of FADD

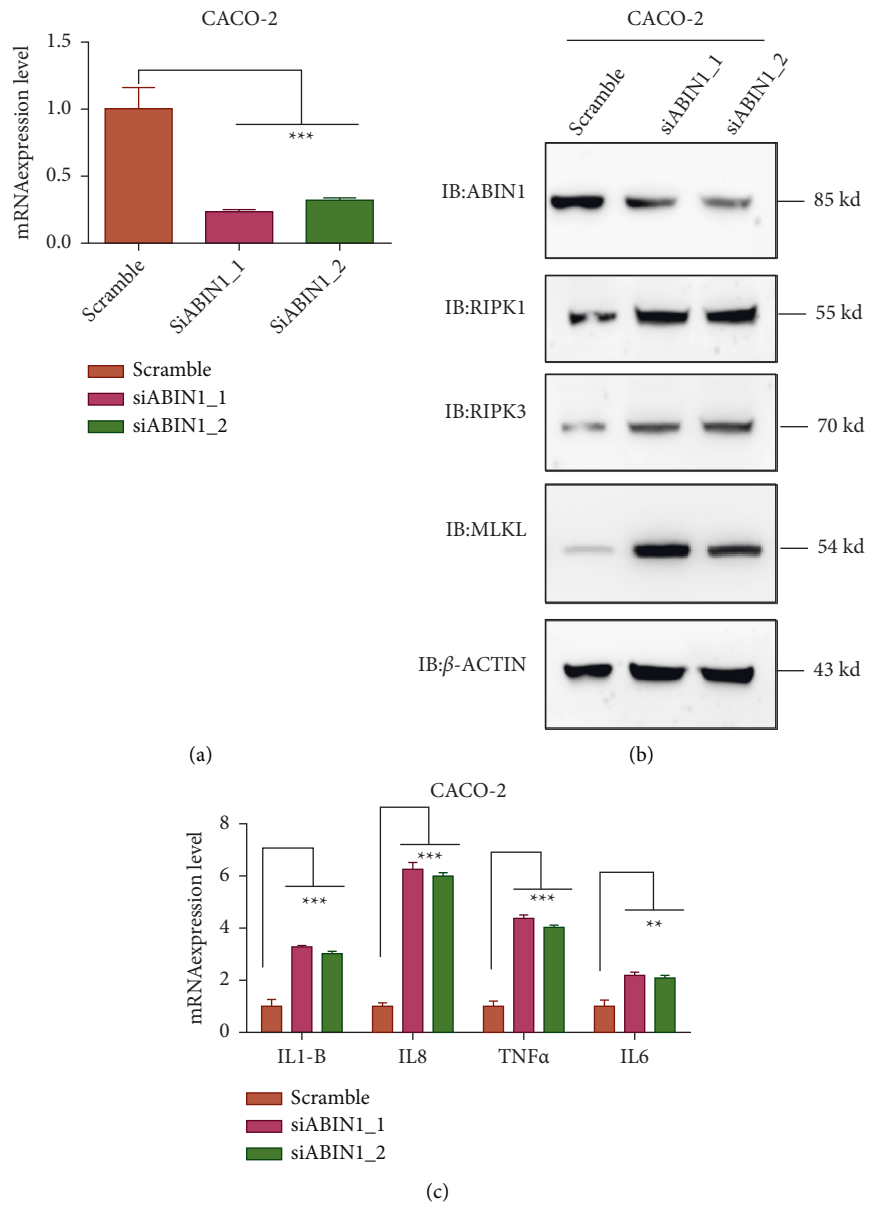

Figure 3: ABIN1 knockdown in IEC promotes necroptosis and the expression of proinflammatory cytokines in IEC. (a) mRNA expression level siRNA verification in CACO-2 cells; (b) Necroptosis-associated proteins detection in CACO-2 ABIN1 knock down stable upon TNF-α stimulation; and (c) ABIN1 knock down CACO-2 cells. Two-tailed Student's t-test was performed to assess statistical significance. $^{**}P < 0.01$, $^{***}P < 0.001$.

based on RIPK1 IEC-KO saved premature death and weight loss in mice, suggesting that loss of RIPK1 gene in IECs leads to FADD-dependent apoptosis and intestinal inflammation [26].

In terms of mechanism research, the connection between RIPK1 and IBD was also reported in 2014. Dannappel et al. [27] found that mice with IECs conditional deletion of RIPK1 gene (RIPK1 IEC-KO) would die within 4 weeks after birth, accompanied by inflammatory infiltration of intestinal tissue. The results were similar to those of RIPK1 IEC-KO mice, indicating that RIPK1 gene not only maintains the homeostasis of newborn mice but also plays a crucial role in adult mice IECs. Belgian Takahashi et al. also reported similar experimental results [28]. They used RIPK1 IEC-KO mice to study and found that Caspase 8 knockout could save the phenotype of RIPK1 IEC-KO mice [29]. Both studies demonstrated that the importance of RIPK1 in the regulation of FADD and Caspase 8 genes in intestinal epidermal cells was consistent with the key regulatory position of RIPK1 protein in the TNF-α signaling pathway [27].

As we know, currently the medical UC therapies were based on traditional 5-aminosalicylate and corticosteroids and new classes of biologic drugs mainly refer to tumor necrosis factor (TNF) antagonists including infliximab, adalimumab, and certuzumab [30]. Compelling evidence shows that anti-TNF therapy remains one of the most

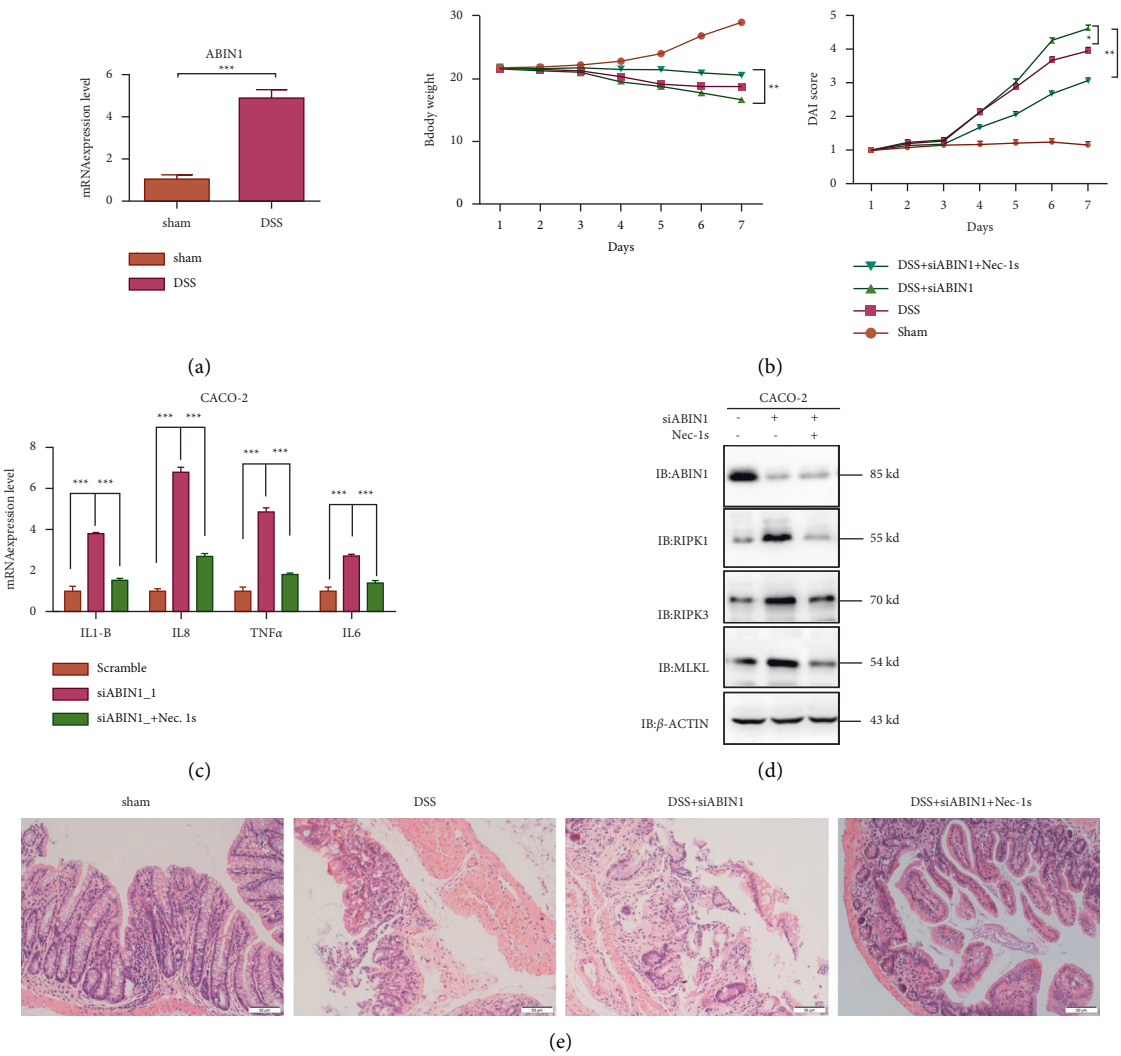

Figure 4: Nec-1s mitigate the necroptosis-associated protein expression and intestinal damage *in vivo and in vitro*. (a) mRNA expression level of ABIN1 in the DSS-induced colitis model; (b) the body weight and DAI index change in mice on combination treatment with DSS, siABIN1 and Nec-1s for 7 days; (c) mRNA expression level of proinflammatory cytokines under ABIN1 ablation and Nec-1s treatment in CACO-2; (d) necroptosis-associated proteins detection expression level under ABIN1 ablation and Nec-1s treatment in CACO-2; and (e) representative images of four groups' colonic tissue stained with hematoxylin and eosin (H&E; upper) are shown. The bar represents 50 μm and two-tailed student's t-test was performed to assess statistical significance. $^{**}P < 0.01$, $^{***}P < 0.001$.

effective ways for treating UC. Furthermore, previous studies shown that the TNF-α signaling pathway was closely related to necroptosis in the absence of caspase 8 [8]. However, the relationship between necroptosis and UC remains largely obscure. In this study, we found that caspase 8 expression level in UC patients' mucosa remarkably decreased compared to healthy patients' mucosa along with the increasing expression of necroptosis-associated protein RIPK1, RIPK3, and MLKL. And the similar results were uncovered in the DSS-induced colitis model. Previous research showed that upon TNF-α stimulation, deficiency of caspase 8 leads to the inhibition of apoptosis and results in the upregulation of RIPK1-RIPK3-MLKL complex II-related necroptosis [31]. It implies that necroptosis plays a main role in the inflammation of UC in a TNF-α-mediating pathway.

ABIN1 is a polyubiquitin-binding protein known to bind linear ubiquitin chains on TNF-RSC and A20 to mediate the deubiquitination of RIPK1 to suppress necroptosis during development [32]. Besides, ABIN1 and A20 are linked to several inflammatory disorders [15, 16]. A20 protein is an anti-inflammatory molecule that inhibits NF-κB inflammatory signaling and cell death downstream of TNF-α. Mutations in its coding genes have been confirmed to be associated with a variety of inflammatory diseases, such as CD and rheumatoid arthritis [33]. In 2018, it was reported that simultaneous conditional knockout of the A20 and ABIN1 genes of IECs led to the failure of mice to survive and the rapid death of IECs. In *in vitro* cell experiments, inhibition of RIPK1 kinase activity by Nec-1s could save the death of IECs cells [34]. Ricard et al. further studied the expression of A20 in IBD patients' tissues, and found that in the ileum and colon of CD patients, A20 is as highly expressed as TNF-α. Upon TNF-α stress, in A20-TG mice and enteroid of A20-TG, IECs cells began to undergo

apoptosis, which was reversed by RIPK1 inhibitor, suggesting that A20 overexpressed intestinal cells which undergo RIPK1-dependent apoptosis by the action of inflammatory factors. In addition, its paralogous gene, ABIN3, shows negatively regulated necroptosis-induced intestinal inflammation by interacting with A20 and restricting the ubiquitination modification of necroptosis in inflammatory bowel disease [31]. So, we investigate the inner function of ABIN1 and RIPK1 in UC. In this study, we found ABIN1 expression level in UC patients' mucosa remarkably increased compared to health mucosa. To further understand the function of ABIN1 in UC, we established the ABIN1 overexpression and knock down in vitro model in CACO-2 cell. We found that overexpression ABIN1 in TNF-α-induced CACO-2 cell leads to the reduction expression of necroptosis core components such as RIPK1, RIPK3, and MLKs. Besides the expression of proinflammatory cytokines including TNF-α, IL-6, IL1B, and IL8 were decreased as well. We knocked down ABIN1 in CACO-2 cell which showed the converse results. And then, we blocked RIPK1 with Nec-1s in the ABIN1 deficiency model which also inhibited the increase of proinflammatory cytokines and necroptosis-associated proteins. Subsequently, we performed *in vivo* experiments to further investigate the role of ABIN1 in UC. We exposed DSS-induced colitis mice with siABIN1/Nec-1s treatment to assess the function of ABIN1 in the UC necroptosis model. Our results showed that with the deficiency of ABIN1, the inflammation that induced by DSS was aggravated, and Nec-1s can restore the effects.

Collectively, our study shows that ABIN1 alleviated UC inflammation through a TNF-stimulation necroptosis-dependent pathway. These results provide insights into UC etiology and suggest that ABIN1 activation may be considered a therapeutic target for treating UC.

Data Availability

All the data can be acquired by reasonable request.

Conflicts of Interest

There are no conflicts of interest.

References

[1] G. G. Kaplan and S. C. Ng, "Understanding and preventing the global increase of inflammatory bowel disease," *Gastroenterology*, vol. 152, no. 2, pp. 313–321, 2017.

[2] G. P. Ramos and K. A. Papadakis, "Mechanisms of disease: inflammatory bowel diseases," *Mayo Clinic Proceedings*, vol. 94, 2019.

[3] J. König, J. Wells, P. D. Cani et al., "Human intestinal barrier function in health and disease," *Clinical and Translational Gastroenterology*, vol. 7, no. 10, p. e196, 2016.

[4] L. W. Peterson and D. Artis, "Intestinal epithelial cells: regulators of barrier function and immune homeostasis," *Nature Reviews Immunology*, vol. 14, no. 3, pp. 141–153, 2014.

[5] A. Negroni, S. Cucchiara, and L. Stronati, "Apoptosis, necrosis, and necroptosis in the gut and intestinal homeostasis," *Mediators of Inflammation*, vol. 2015, Article ID 250762, 10 pages, 2015.

[6] M. Pasparakis and P. J. N. Vandenabeele, "Necroptosis and its role in inflammation," *Nature*, vol. 517, no. 7534, pp. 311–320, 2015.

[7] R. Weinlich, A. Oberst, H. M. Beere, and D. R. Green, "Necroptosis in development, inflammation and disease," *Nature Reviews Molecular Cell Biology*, vol. 18, no. 2, pp. 127–136, 2017.

[8] N. Holler, R. Zaru, O. Micheau et al., "Fas triggers an alternative, caspase-8–independent cell death pathway using the kinase RIP as effector molecule," *Nature Immunology*, vol. 1, no. 6, pp. 489–495, 2000.

[9] Y. Ito, D. Ofengeim, A. Najafov et al., "RIPK1 mediates axonal degeneration by promoting inflammation and necroptosis in ALS," *Science*, vol. 353, no. 6299, pp. 603–608, 2016.

[10] D. Ofengeim, Y. Ito, A. Najafov et al., "Activation of necroptosis in multiple sclerosis," *Cell Reports*, vol. 10, no. 11, pp. 1836–1849, 2015.

[11] J. Wong, R. Garcia-Carbonell, M. Zelic et al., "RIPK1 mediates TNF-induced intestinal crypt apoptosis during chronic NF-κB activation," *Cellular and Molecular Gastroenterology and Hepatology*, vol. 9, no. 2, pp. 295–312, 2020.

[12] S. A. Dziedzic, Z. Su, V. Jean Barrett et al., "ABIN-1 regulates RIPK1 activation by linking Met1 ubiquitylation with Lys63 deubiquitylation in TNF-RSC," *Nature Cell Biology*, vol. 20, no. 1, pp. 58–68, 2018.

[13] M. Onizawa, S. Oshima, U. Schulze-Topphoff et al., "The ubiquitin-modifying enzyme A20 restricts ubiquitination of the kinase RIPK3 and protects cells from necroptosis," *Nature Immunology*, vol. 16, no. 6, pp. 618–627, 2015.

[14] S. Oshima, E. E. Turer, J. A. Callahan et al., "ABIN-1 is a ubiquitin sensor that restricts cell death and sustains embryonic development," *Nature*, vol. 457, no. 7231, pp. 906–909, 2009.

[15] J. A. Callahan, G. E. Hammer, A. Agelides et al., "Cutting edge: ABIN-1 protects against psoriasis by restricting MyD88 signals in dendritic cells," *The Journal of Immunology*, vol. 191, no. 2, pp. 535–539, 2013.

[16] D. J. Caster, E. A. Korte, S. K. Nanda et al., "ABIN1 dysfunction as a genetic basis for lupus nephritis," *Journal of the American Society of Nephrology*, vol. 24, no. 11, pp. 1743–1754, 2013.

[17] W. Xu, Y. Guo, Z. Huang et al., "Small heat shock protein CRYAB inhibits intestinal mucosal inflammatory responses and protects barrier integrity through suppressing IKKβ activity," *Mucosal Immunology*, vol. 12, no. 6, pp. 1291–1303, 2019.

[18] N. Takahashi, L. Duprez, S. Grootjans et al., "Necrostatin-1 analogues: critical issues on the specificity, activity and in vivo use in experimental disease models," *Cell Death & Disease*, vol. 3, no. 11, p. e437, 2012.

[19] B. Z. Stanger, P. Leder, T. H. Lee, E. Kim, and B. Seed, "RIP: a novel protein containing a death domain that interacts with Fas/APO-1 (CD95) in yeast and causes cell death," *Cell*, vol. 81, no. 4, pp. 513–523, 1995.

[20] A. T. Ting, F. X. Pimentel-Muiños, and B. Seed, "RIP mediates tumor necrosis factor receptor 1 activation of NF-κB but not Fas/APO-1-initiated apoptosis," *The EMBO Journal*, vol. 15, no. 22, pp. 6189–6196, 1996.

[21] A. Degterev, Z. Huang, M. Boyce et al., "Chemical inhibitor of nonapoptotic cell death with therapeutic potential for ischemic brain injury," *Nature Chemical Biology*, vol. 1, no. 2, pp. 112–119, 2005.

[22] M. A. Kelliher, S. Grimm, Y. Ishida, F. Kuo, B. Z. Stanger, and P. Leder, "The death domain kinase RIP mediates the TNF-

induced NF-κB signal," *Immunity*, vol. 8, no. 3, pp. 297–303, 1998.

[23] A. Polykratis, N. Hermance, M. Zelic et al., "Cutting edge: RIPK1 Kinase inactive mice are viable and protected from TNF-induced necroptosis in vivo," *The Journal of Immunology*, vol. 193, no. 4, pp. 1539–1543, 2014.

[24] D. Cuchet-Lourenço, D. Eletto, C. Wu et al., "Biallelic RIPK1 mutations in humans cause severe immunodeficiency, arthritis, and intestinal inflammation," *Science*, vol. 361, no. 6404, pp. 810–813, 2018.

[25] L. Lin, Y. Wang, L. Liu et al., "Clinical phenotype of a Chinese patient with RIPK1 deficiency due to novel mutation," *Genes & Diseases*, vol. 7, no. 1, pp. 122–127, 2020.

[26] N. Lalaoui, S. E. Boyden, H. Oda et al., "Mutations that prevent caspase cleavage of RIPK1 cause autoinflammatory disease," *Nature*, vol. 577, no. 7788, pp. 103–108, 2020.

[27] M. Dannappel, K. Vlantis, S. Kumari et al., "RIPK1 maintains epithelial homeostasis by inhibiting apoptosis and necroptosis," *Nature*, vol. 513, no. 7516, pp. 90–94, 2014.

[28] N. Takahashi, L. Vereecke, M. J. M. Bertrand et al., "RIPK1 ensures intestinal homeostasis by protecting the epithelium against apoptosis," *Nature*, vol. 513, no. 7516, pp. 95–99, 2014.

[29] D. E. Christofferson, Y. Li, and J. Yuan, "Control of life-or-death decisions by RIP1 kinase," *Annual Review of Physiology*, vol. 76, no. 1, pp. 129–150, 2014.

[30] P. Hindryckx, N. Vande Casteele, G. Novak et al., "The expanding therapeutic armamentarium for inflammatory bowel disease: how to choose the right drug [s] for our patients?" *Journal of Crohn's and Colitis*, vol. 12, no. 1, pp. 105–119, 2018.

[31] M. Zhou, J. He, Y. Shi et al., "ABIN3 negatively regulates necroptosis-induced intestinal inflammation through recruiting A20 and restricting the ubiquitination of RIPK3 in inflammatory bowel disease," *Journal of Crohn's and Colitis*, vol. 15, no. 1, pp. 99–114, 2021.

[32] S. A. Dziedzic, Z. Su, V. Jean Barrett et al., "ABIN-1 regulates RIPK1 activation by bridging M1 ubiquitination with K63 deubiquitination in TNF-RSC," *Nature Cell Biology*, vol. 20, 2017.

[33] D. Priem, G. Van Loo, and M. Bertrand, "A20 and cell death-driven inflammation," *Trends in Immunology*, vol. 41, no. 5, pp. 421–435, 2020.

[34] L. Vereecke, S. Vieira-Silva, T. Billiet et al., "A20 controls intestinal homeostasis through cell-specific activities," *Nature Communications*, vol. 5, no. 1, pp. 5103–5112, 2014.

Hindawi
Genetics Research
Volume 2022, Article ID 1831211, 12 pages
https://doi.org/10.1155/2022/1831211

Research Article

Comprehensive Analysis of Genomic and Expression Data Identified Potential Markers for Predicting Prognosis and Immune Response in CRC

Yongshan He, Xuan Dai, Yuanyuan Chen, and Shiyong Huang

Department of Colorectal Surgery, Xinhua Hospital Affiliated to Shanghai Jiaotong University, School of Medicine, No. 1665 Kongjiang Road, Shanghai 200092, China

Correspondence should be addressed to Shiyong Huang; huangshiyong@xinhuamed.com.cn

Received 24 March 2022; Revised 22 June 2022; Accepted 23 June 2022; Published 30 July 2022

Academic Editor: Ying-Kun Xu

Colorectal cancer (CRC) is the most prevalent type of malignant tumor of the gastrointestinal tract. In the current study, we characterized the landscape of genomic alterations in CRC patients. Based on the results of whole-exome sequencing (WES), we identified 31 significantly mutated genes. Among them, several genes including TP53, KRAS, APC, PI3KCA, and BRAF were reported as significantly mutated genes in previous studies. In the current study, the most frequently mutated gene was TP53, which encodes tumor suppressor p53, affecting approximately 60% of CRC patients. In addition, we performed the expression profiles of significantly mutated genes between the normal group and tumor groups and identified 20 differentially expressed genes (DEGs); among them, CSMD3, DCHS2, LRP2, RYR2, and ZFHX4 were significantly negatively correlated with PFS. Moreover, consensus clustering analysis for CRC based on the expression of significantly somatic mutated genes was performed. In total, three subtypes of CRC were identified in CRC, including cluster1 ($n = 453$), cluster2 ($n = 158$), and cluster 3 ($n = 9$), based on expression level of significantly somatic mutated genes. Clinicopathological features analysis showed subtype C1 had the longest progression-free survival (PFS) with median time of 8.2 years, while subtypes C2 and C3 had 4.1 and 2.7 years of PFS, respectively. Moreover, we found three subtypes related to tumor infiltration depth, lymph node metastasis, and distant metastasis. Immune infiltration analysis showed the tumor infiltration levels of B cell native, T cell CD8+, T cell CD4+ memory activated, T cell gamma delta, NK cell resting, macrophage M0, macrophage M2, myeloid dendritic cell activated, mast cell activated, and mast cell resting significantly changed among the three groups, demonstrating the three subgroups classified by 22 somatically significantly mutated genes had a high capacity to differentiate patients with different immune statuses, which is helpful for the prediction of immunotherapy response of CRC patients. Our findings could provide novel potential predictive indicators for CRC prognosis and therapy targets for CRC immunotherapy.

1. Introduction

Colorectal cancer is the most prevalent type of malignant tumor of the gastrointestinal tract [1]. In 2020, colorectal cancer is the third most common cancer, with more than 193000 diagnosed cases [2], leading to the second cause of cancer-related deaths, with around 830000 fatalities. Studies have found that nearly 50% of colorectal cancer patients will eventually have distant metastases, and the resistance of colorectal cancer to chemotherapy drugs has led to treatment failure and tumor metastasis invasion [3]. Immunotherapy, in addition to surgery and chemotherapy, has been identified as a promising treatment for specific subtypes of CRC [4]. However, there were differences in prognosis amongst patients with the same disease stage, which were linked to distinct genetic abnormalities, underlining CRC's molecular heterogeneity.

The human immune system will go through three stages of tumor development: immune clearance, immune balance, and immune escape [5]. Based on this theory, immunotherapy plays a role to restore or enhance the antitumor effect of the immune system. With the development of

tumor cytology, immunotherapy has been paid more and more attention in the treatment of malignant tumors and has achieved good efficacy in some subtypes of colorectal cancer patients [6]. Currently, the research related to immune checkpoint inhibitors is relatively mature and widely used in tumor immunotherapy. Immunotherapy drugs primarily target PD-1, PD-L1, and CTLA-4 [7]. At present, PD-1/PD-L1 inhibitors are relatively commonly used in the immunotherapy of colorectal cancer, and their efficacy is relatively favorable in patients with deficient mismatch repair (dMMR) or microsatellite instability-high (MSI-H) types, and the efficacy in patients with other subtypes needs to be further explored, in which the level of PD-L1 expression may have an impact on the efficacy [8]. However, mismatch repair proficient (MMR) or microsatellite stable (MSS) types account for the majority of patients with colorectal cancer. In recent years, some researchers have begun to focus on the immune escape mechanism of pMMR/MSS colorectal cancer, trying to convert its immune "cold environment" into a "hot environment." Recent advances in genomics and bioinformatics have facilitated identification of new immune-related genes through cancer genome sequencing [9]. Therefore, it is promising to develop a novel genomic and expression-based classification of CRC with an improved clinical significance.

In this study, we compared gene expression differences between wild-type genes and mutant genes using expression profiles and genomic data, as well as performed Cox regression analysis. In addition, bioinformatics analysis was employed to investigate the clinical profile and distinct characteristics of immunogenicity of different subtypes of CRC. Our findings could provide novel potential predictive indicators and therapy targets for CRC immunotherapy.

2. Materials and Methods

2.1. Data Acquisition. TCGA database (https://portal.gdc.cancer.gov/) was used to extract mutational data, RNA-seq data, and clinical medical information of CRC patients. Our study included a total of 536 CRC samples, which included 536 CRC tumor samples and 536 adjacent normal samples.

2.2. Unsupervised Consensus Clustering Analysis. Using the Consensus Cluster Plus R package, we conducted an unsupervised consensus analysis [10]. In a brief, a graph of the consistency matrix based on the k value is displayed. Furthermore, for each k, the empirical cumulative distribution function plot shows a uniform distribution. The cluster consensus graph depicts the cluster consensus values for various k values. A higher cluster consensus value indicates a lower level of cluster stability. The average consensus value is drawn from a project and members of a consensus cluster are represented by a project consensus graph. Multiple project consensus values with varying k values are displayed in a project.

2.3. Immune Signature Analysis in Molecular Subtypes. The ESTIMATE algorithm was used to calculate expression scores for microenvironmental factors [11]. Tumor samples were analyzed with TIMER [12] for six tumor-infiltrating lymphocytes, including CD8+ T cells, dendritic cells, neutrophils, B cells, macrophages, and CD4+ T cells. Heatmaps were used to visualize the expression scores for immune signatures in different subgroups of CRC. Immune signatures and checkpoint gene expression levels were also examined across all molecular subtypes.

2.4. Differentially Expressed Gene Analysis. DEGs between different clusters of CRC were determined by Student's t-test, observing cutoff values $|\log2 \text{ (fold change)}| > 1$ and p values <0.05.

3. Results

3.1. The Landscape of Somatic Mutations of CRC. 536 WES samples data were conducted to analyze the landscape of somatic mutations of CRC. There were 525 samples (97.95%) altered in a total of 536 samples (Figure 1(a)). In addition, 31 genes were identified as significantly mutated genes including APC, TP53, KRAS, PIK3CA, TNN, SYNE1, MUC16, FAT4, RYR2, OBSCN, ZFHX4, LRP1B, DNAH5, DNAH11, FAT3, CSMD3, FBXW7, PCLO, CSMD1, ABCA13, USH2A, RYR1, FLG, NEB, RYR3, ADGRV1, LRP2, CCDC168, DCHS2, ATM, and A1BG (Figure 1(a)). The variant classification can be divided into 9 types, among which missense mutations account for the majority (Figures 1(b) and 1(c)). The predominant somatic mutation types were $C > T$ (Figure 1(d)). The median variants per sample were 106. TTN, APC, MUC16, SYNE1, TP53, FAT4, KARS, RYR2, OBSCN, and PIK3CA were the top 10 mutant genes (Figures 1(e) and 1(g)).

3.2. Identification of Survival-Associated Somatic Mutated Genes. To investigate the link between somatic mutations and CRC prognosis, 31 significantly mutated genes were divided into two groups, respectively. We identified 4 genes SYNE1, TNN, CCDC168, and NEN mutations were significantly related to short overall survival (Figures 2(a)–2(d)). In addition, we performed the expression profiles of significantly mutated genes in one normal group and two tumor groups. We found that 20 genes were dramatically changed between the normal colon tissue and tumor group (Figure 3(a)). Among them, DNAH5, TP53, OBSCN, LRP2, NEB, PCLO, MUC16, USH2A, and CCDC168 were significantly upregulated. CSMD1, SYNE1, RYR1, RYR3, APC, ADGRV1M, DCHS2, KRAS, LRP1B, and FAT4 were significantly downregulated (Figure 3(a)) Furthermore, the relationship between the expression of somatically mutated genes and progression-free survival (PFS) in CRC was investigated. We identified high expressions of CSMD3, DCHS2, LRP2, RYR2, and ZFHX4 were significantly negatively correlated with PFS in CRC (Figures 3(b)–3(f)).

3.3. Consensus Clustering Analysis for CRC Based on the Expression of Significantly Somatic Mutated Genes.

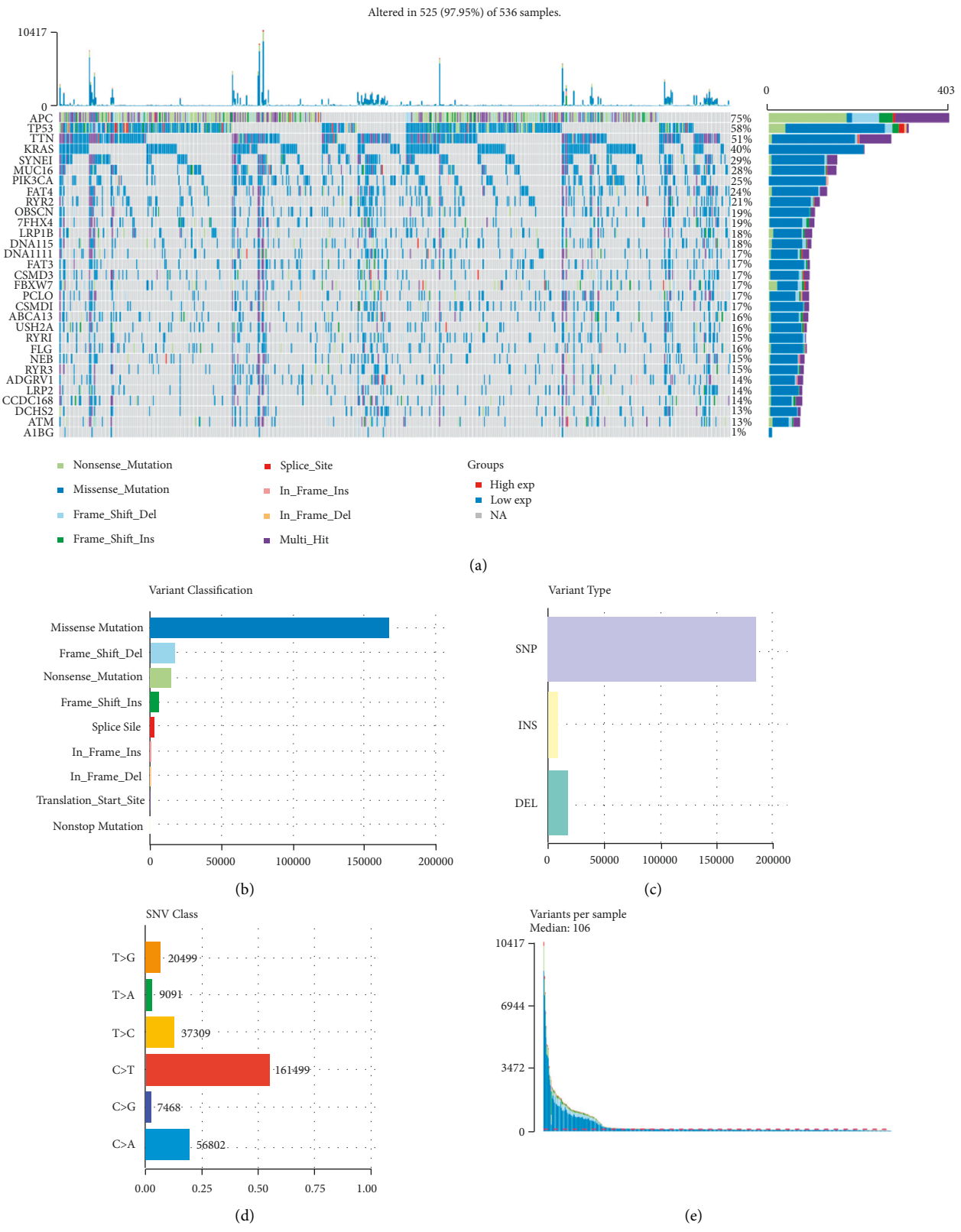

Figure 1: Continued.

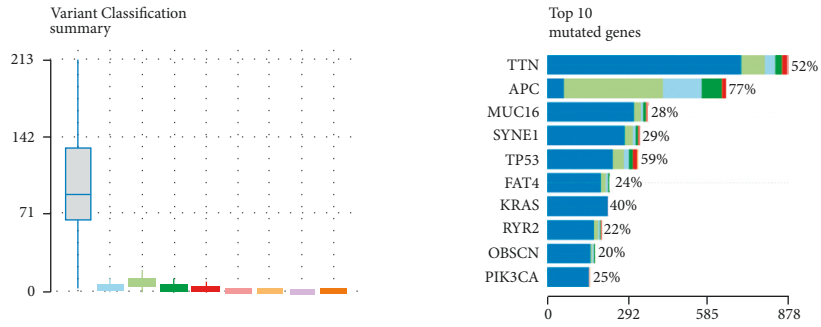

(f) (g)

Figure 1: Landscape of somatic mutations of CRC. (a) Oncoplot and waterfall plot showing the somatic landscape of top 31 mutated genes in CRC. The distribution of variant classification (b), variant type (c), and SNV class (d) present. (e)-(f) Mutation load of each sample (variant classification type), and stacked bar graph shows the top ten mutated genes, including TTN, APC, MUC16, SYNE1, TP53, FAT4, KARS. RYR2, OBSCN, and PIK3CA.

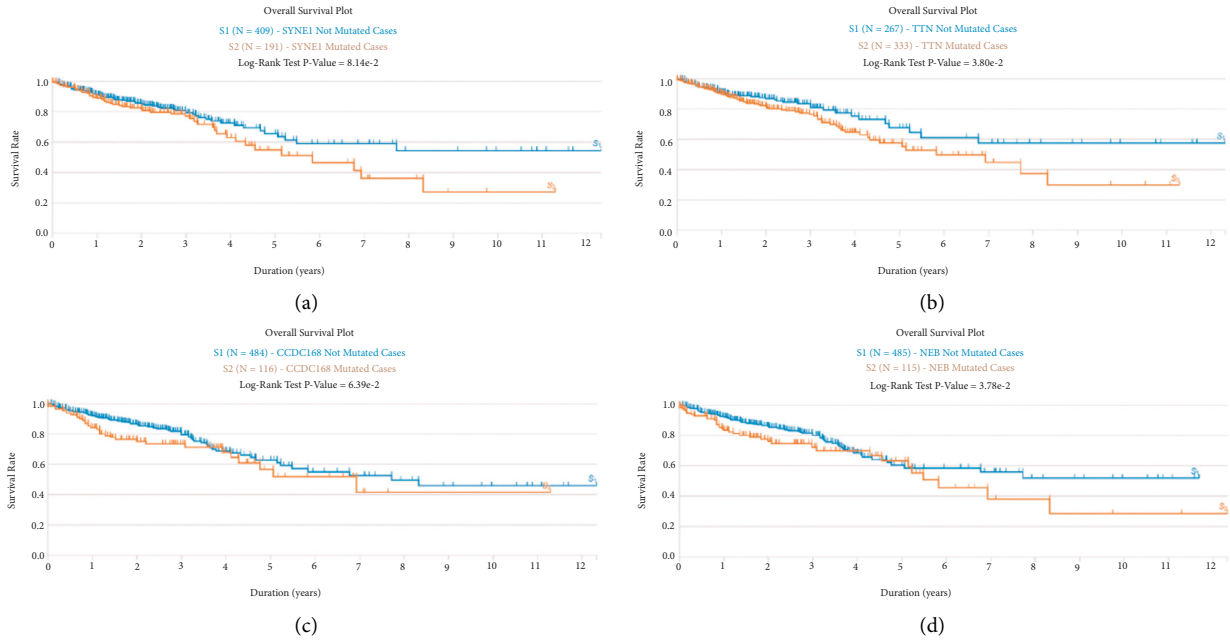

Figure 2: Identification of survival-associated somatic mutated genes. The CRC patients with SYNE1 (a), TNN (b), CCDC168 (c), and NEN (d) mutations had a shorter overall survival time.

Consensus clustering was performed using the Consensus Cluster Plus R program. At consensus index, with $k = 3$, the cumulative distribution function has the lowest rangeability (Figure 4(a)). At $k = 3$, the analysis had the best delta area scores (Figure 4(b)). In total, three subtypes of CRC were identified in 620 CRC samples, including cluster1 ($n = 453$), cluster2 ($n = 158$), and cluster 3 ($n = 9$) based on expression level of significantly somatic mutated genes (Figures 4(c) and 4(d)). Our data show that clustered subtypes defined by the expression level of somatically mutated genes are closely related to the heterogeneity of CRC patients (Figure 5(a)).

3.4. Clinicopathological Features Analysis of Somatically Mutated Genes Related Subgroups of CRC. Unsupervised clustering based on subgroups formed from mutational signatures and critical gene changes was carried out to establish genomic categorization of CRC linked with patients' clinical and pathological features and progression-free survival. As shown in Figure 5(b), subtype C1 had the longest PFS with a median time of 8.2 years, while subtypes C2 and C3 had 4.1 and 2.7 years PFS, respectively. In addition, we found that three subtypes related to the grade and metastasis stage. Subtype C1 contains more early stage, subtype C2 is intermediate malignancy, while subtype 3 has the greatest malignancy (Figures 5(c)–5(f)).

3.5. Association between Immune Infiltration and Genomic Consensus Cluster in CRC. In subtyping analysis, we compared the immune infiltration of the three subgroups by the CIBERSORT algorithm. We found that B cell native, T cell

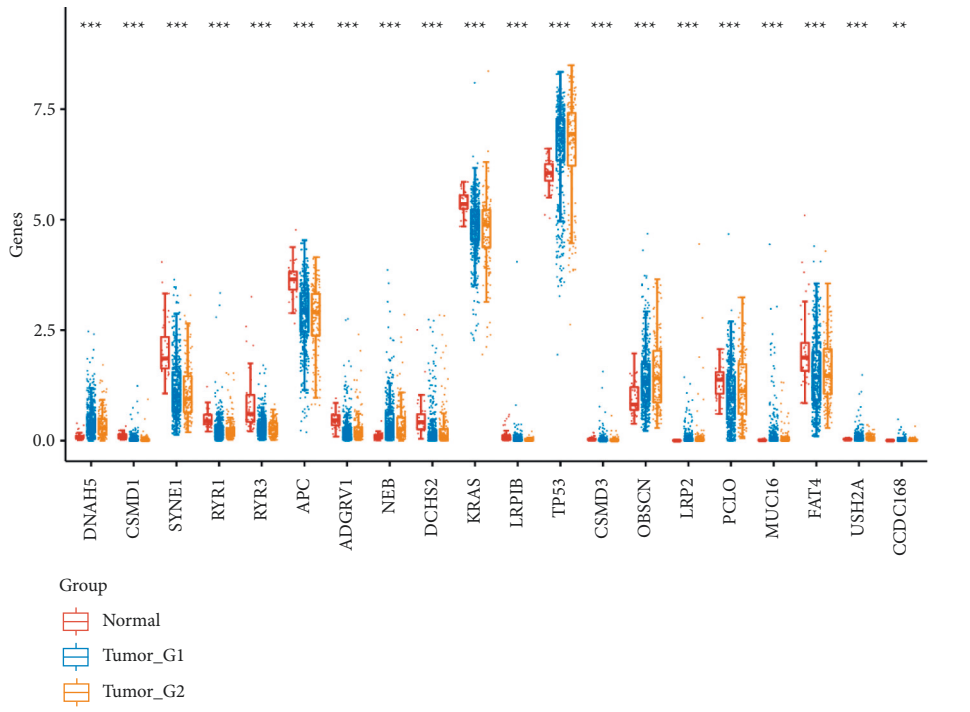

(a)

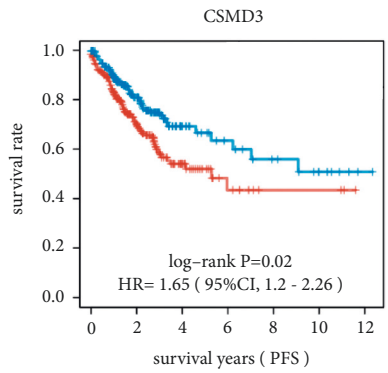

(b)

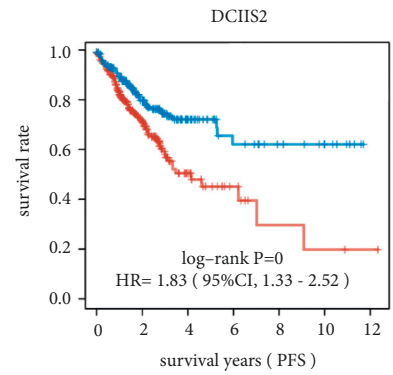

(c)

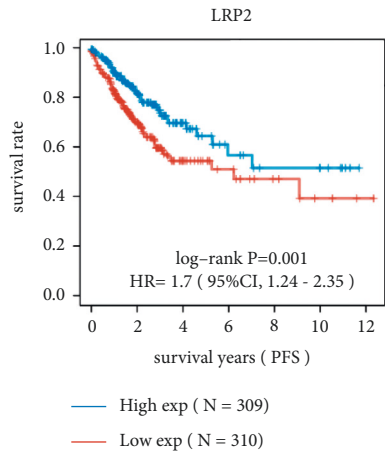

(d)

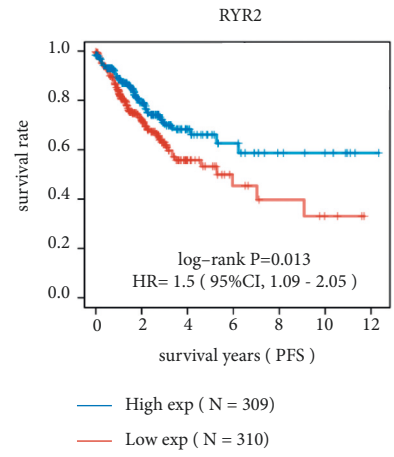

(e)

Figure 3: Continued.

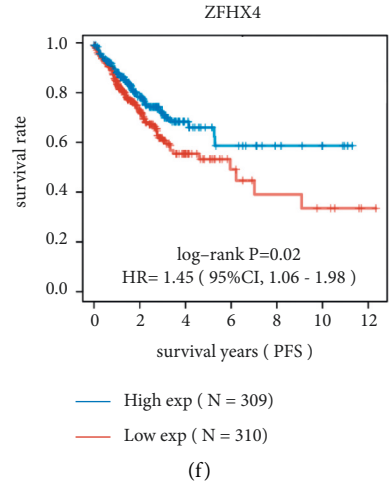

Figure 3: The dysregulation of somatically mutated genes was correlated to the prognosis of CRC. (a) 20 genes dramatically changed between the normal colon tissue and CRC group. Among them, DNAH5, TP53, OBSCN, LRP2, NEB, PCLO, MUC16, USH2A, and CCDC168 significantly upregulated. CSMD1, SYNE1, RYR1, RYR3, APC, ADGRV1M, DCHS2, KRAS, LRP1B, and FAT4 significantly downregulated. High expression of CSMD3 (b), DCHS2 (c), LRP2 (d), RYR2 (e), and ZFHX4 (f) significantly negatively correlated with shorter PFS in CRC.

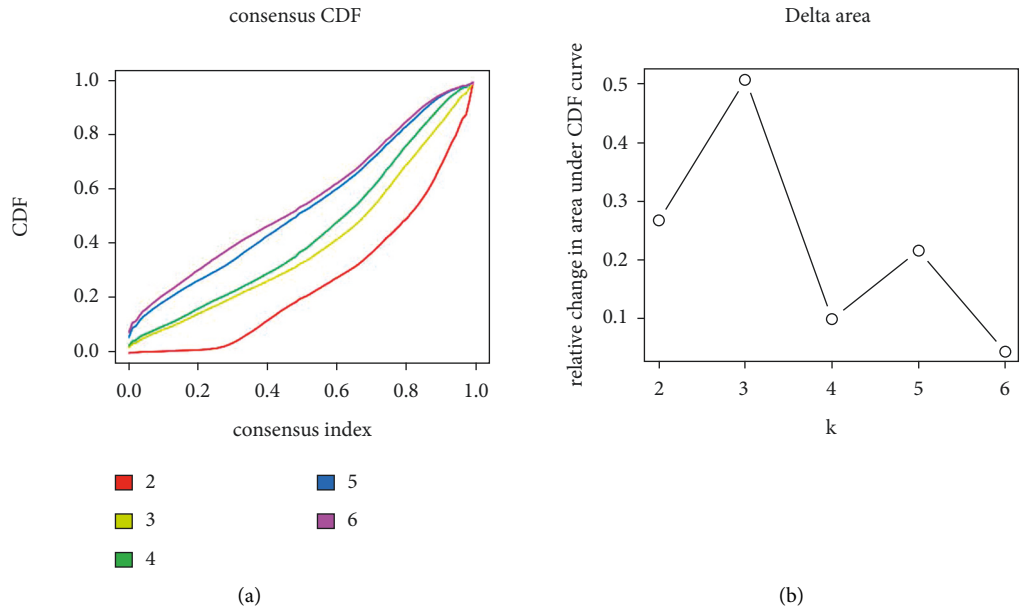

Figure 4: Continued.

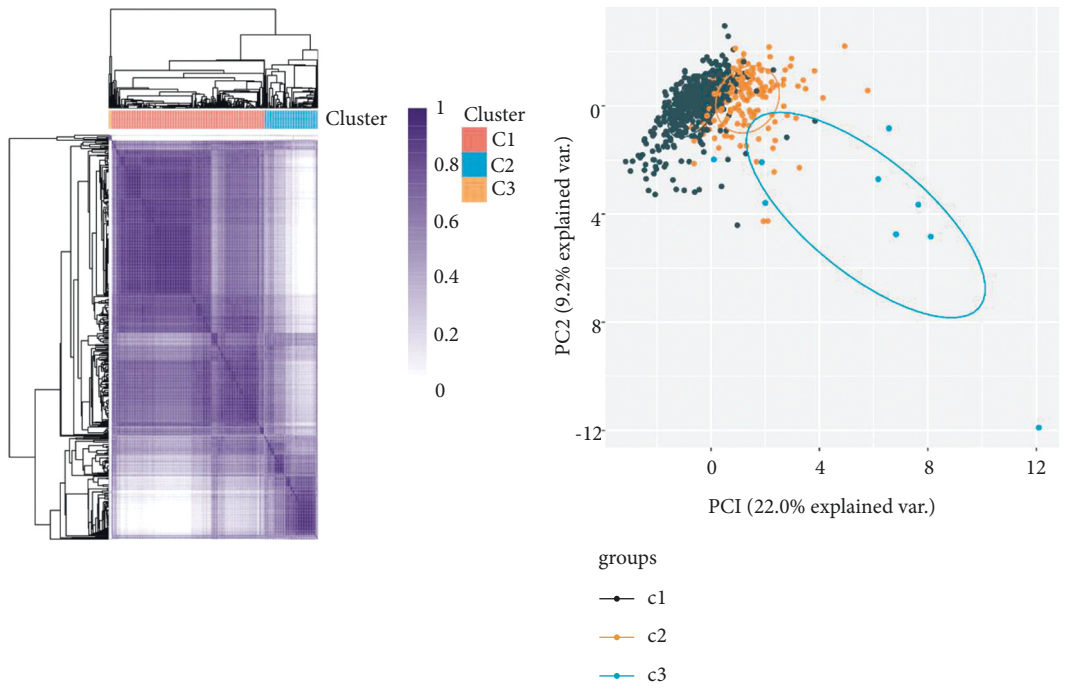

(c) (d)

Figure 4: Consensus clustering analysis for CRC based on the expression of significantly somatic mutated genes. (a) The cumulative distribution function analysis of CRC subtypes. (b) Relative change in the area under the CDF curve (CDF delta area) presented. At $k = 3$, the analysis had the best delta area scores. (c) Three subtypes of CRC identified in CRC samples. (d) The PCA analysis of three subtypes of CRC performed.

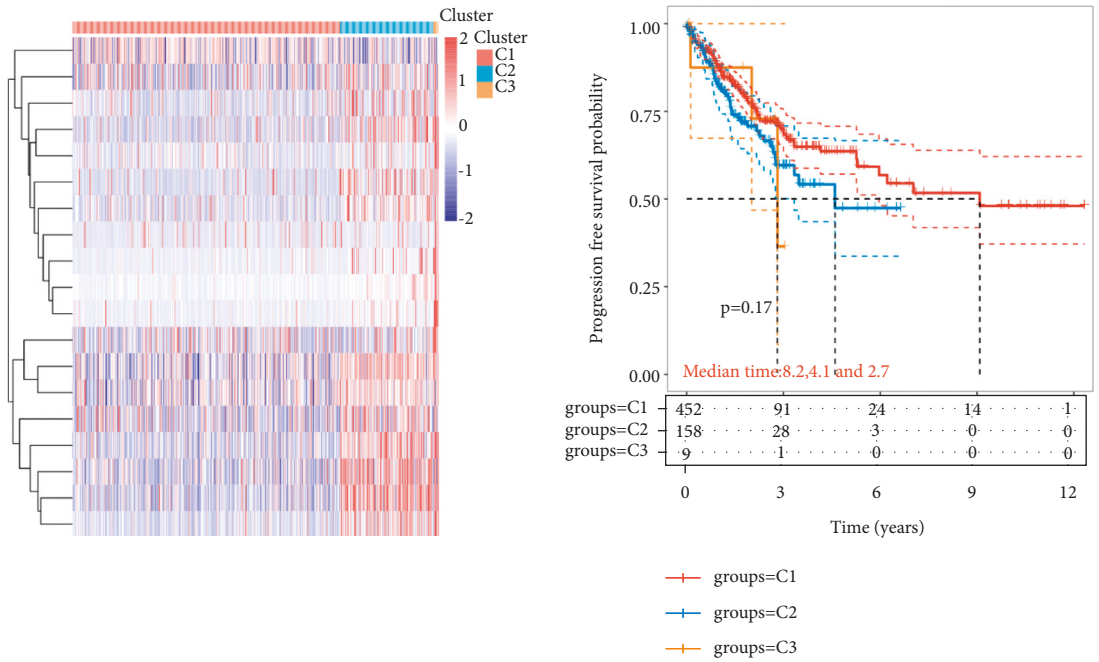

(a) (b)

Figure 5: Continued.

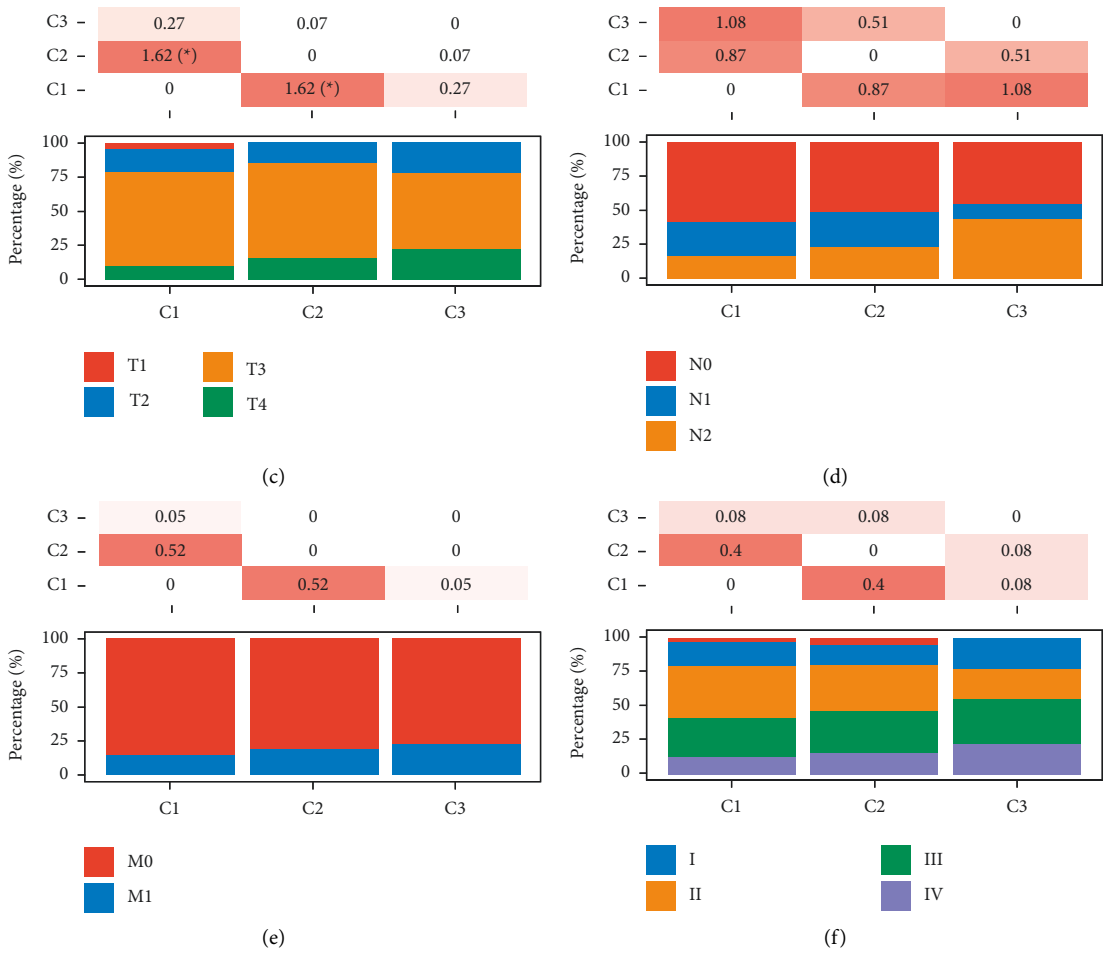

Figure 5: Clinicopathological features analysis of somatically mutated genes related subgroups of CRC. (a) Heatmap showing the expression levels of somatically mutated genes in subgroups of CRC. (b) Kaplan–Meier survival analysis of the correlation between subgroups and PFS time in CRC. (c) The distribution analysis of T stage in different subgroups of CRC. (d) The distribution analysis of N stage in different subgroups of CRC. (e) The distribution analysis of M stage in different subgroups of CRC. (f) The distribution analysis of grades in different subgroups of CRC.

CD8+, T cell CD4+ memory activated, T cell gamma delta, NK cell resting, macrophage M0/M2, myeloid dendritic cell activated, mast cell activated, and mast cell resting had differences among the three groups (Figure 6).

Additionally, a higher number of B cell native were produced in subtype C3 than in other subtypes; T cell CD4+ memory resting/activated and NK cell resting were significantly lower in C3 than in C1 and C2 subtypes; macrophage M0/M2, myeloid dendritic cell activated, and mast cell activated were significantly higher in C2 than in C1 and C3 subtypes; interestingly, mast cell resting was significantly lower in C2 than in C1 and C3 subtypes (Figures 6(a) and 6(b)).

4. Discussion

In the current study, we characterized the landscape of genomic alterations in CRC patients. Based on the results of WES, we identified 31 significantly mutated genes. Among them, several genes including TP53, KRAS, APC, PI3KCA, and BRAF were reported as significantly mutated genes in previous studies. In the current study, the most frequently mutated gene was TP53, which encodes tumor suppressor p53, affecting approximately 60% of CRC patients. A previous study showed that loss of p53 transcriptional activity leads to uncontrolled cell growth in various organs, including the colon [13]. In addition, KRAS mutations are the main intestinal cancer markers. Studies showed that 30% of human malignant tumors were related to KRAS gene mutation. The mutated KRAS is activated and unable to create normal RAS protein, causing the intracellular signal to be disrupted, resulting in uncontrolled cell proliferation and cancer [14]. Furthermore, mutations in the APC gene are the molecular pathological basis of adenomatous polyposis (FAP) and play a crucial role in the development of sporadic colorectal cancer [15]. APC protein deficiency results in β-catenin accumulation in the cytoplasm; this leads to sustained transcriptional activation of TCF-mediated genes and promotes colorectal cancer progression [16]. BRAF mutations are observed in 8–12% of patients with advanced disease, and a valine amino acid substitution (V600E) in exon 15 is the most common alteration. BRAF mutations in

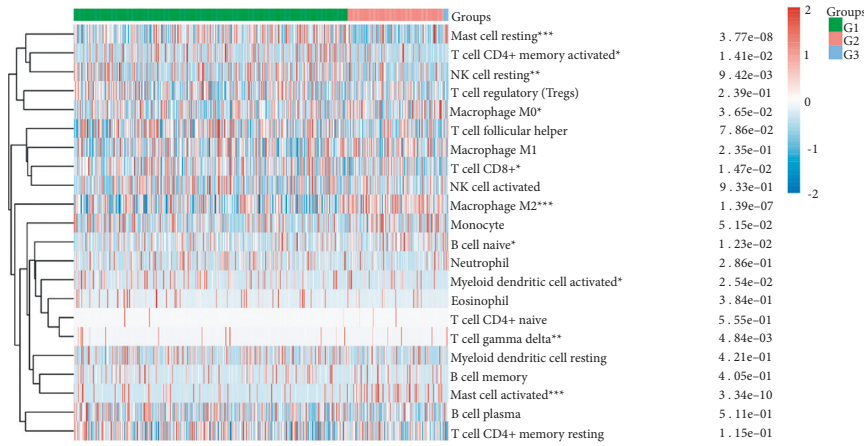

(a)

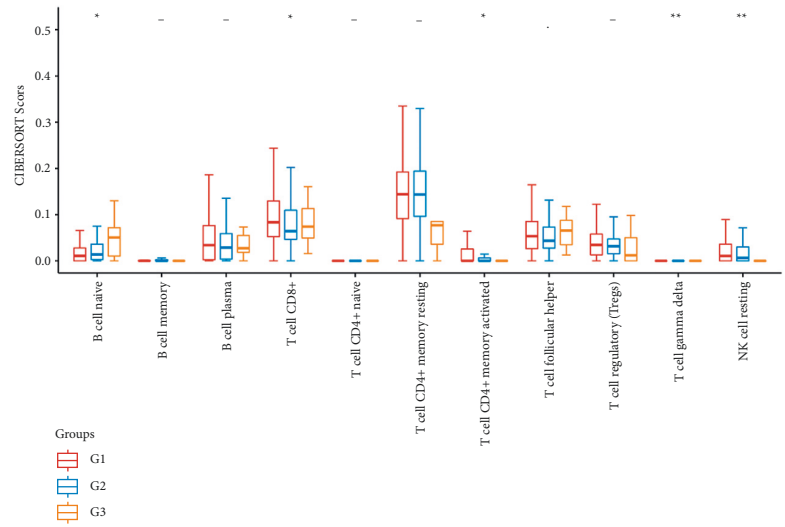

(b)

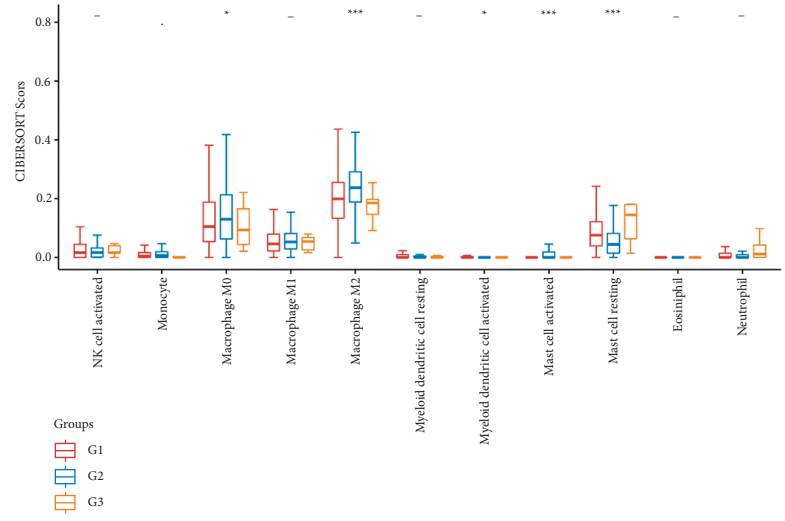

(c)

Figure 6: Association between immune infiltration and genomic consensus cluster in CRC. (a) Heatmap analysis showing immune infiltration of immune cells in three subgroups by the CIBERSORT algorithm. (b) Box-plot analysis showing immune infiltration levels in three subgroups by the CIBERSORT algorithm.

CRC cause MAPK/ERK signaling abnormal activation, which affects cell growth and differentiation pathways [17]. Mutations in the PIK3CA gene cause the creation of an altered p110 subunit, which permits PI3K to hypersignal without being regulated, triggering malignant cell actions such as proliferation and migration [18]. In addition to these commonly mutated genes, genomic mutations in SYNE1, TTN, NEB, and CCDC168 were found to be associated with a poor prognosis of colorectal cancer in this study. SYNE1 encodes a spectrin repeat-containing protein Nesprin-1 that localizes to the nuclear membrane. Mutation of SYNE1 in exonic rs9479297 leads to the upregulation of proteins SYNE1, which may contribute to cell proliferation and migration in hepatocellular and transitional cell carcinoma [19]. Loss of Nesprin-1 in CRC cells may alter cell destiny, contributing to carcinogenesis. In our study, somatic-mutated SYNE1 cases displayed a worse overall survival. Djulbegovic et al. demonstrated that in ocular surface squamous neoplasia, this gene mutation is the most common genetic abnormality. TTN mutations are also linked to resistance to topical interferon alpha-2b (IFN-2b) therapy, which promotes chromosomal instability, oncogenesis, and a changed response to IFN-2b treatment. Xie et al. discovered that TTN mutation was enriched in samples with high immunostimulatory signatures and that the mutation load within TTN implies high TMB status, which is consistent with our finding that somatically mutated TTN cases had a lower overall survival [20]. NEB encodes nebulin, a giant protein component of the cytoskeletal matrix. In taxol-resistant ovarian cancer cells, NEB along with DCDC2, ANKRD18B, ALDH1A1, and ITGBL1 were overexpressed suggesting the involvement of these AR-related genes in taxol resistance. NEB was also identified as a potential cancer-related gene, but research into NEB in CRC is still in its early stages. In our study, we demonstrate that NEB-mutated cases are associated with the worse overall survival in CRC patients.

In addition, we performed the expression profiles of significantly mutated genes in one normal group and two tumor groups; we identified 20 DEGs; among them CSMD3, DCHS2, LRP2, RYR2, and ZFHX4 were significantly negatively correlated with PFS. Lu et al. discovered that CSMD3 is linked to tumor mutation burden and immune infiltration in ovarian cancer patients [21] and was identified as a potential driver gene in prostate adenocarcinoma. However, it is unclear whether CSMD3 is a driver protein in CRC and how CSMD3 contributed to tumorigenesis. DCHS2 is a big protein with numerous cadherin domains that are thought to play a role in cell adhesion. This gene may be relevant in the stomach and colorectal malignancies with high microsatellite instability, according to genome-wide association studies. It suggests that DCHS2 may relate to the immune response of MSI-H [22]. LRP2/megalin was one of the first endocytic cargos identified for the Dab2 adaptor and has been found related to poor prognosis in various cancer. In thyroid tumors, LRP2 mediated the suppressive effect of metformin on cancer proliferation by blocking JNK signaling [23]. LRP2/megalin expression influences melanoma cell growth and survival rates in frequently acquired melanoma tumors [24]. In addition, LRP2 was reported to relate to fibrosis-associated diseases and cancer through the TGF-β pathway. Furthermore, RYR2 is an important player in steroid metabolism and cancer research. Several studies uncovered that RYR2 mutation played a positive side in tumor prognosis. Wei et al. found that RYR2 3′UTR polymorphisms remained significant in the genetic susceptibility of progesterone receptor positive breast cancer [25]. Liu et al. found the RYR2 mutation was linked to a greater TMB and a better clinical outcome by enhancing the antitumor immune response in breast cancer and esophageal adenocarcinoma [26]. In nonsmall cell lung cancer, RYR2 mutation may prolong survival via downregulation of DKK1 and upregulation [27]. In this study, we found that RYR2 expression was negatively related to the PFS in CRC. We speculate that the heterogeneity that exists between tumors causes RYR2 to exhibit different functions in colorectal cancer or due to the insufficient sample size of the analyzed data. ZFHX4 is a 397 kD putative transcription factor with 4 homeodomains and 22 zinc fingers that were discovered lately [28]. Chudnovsky et al. reported ZFHX4 interacts with CHD4 to govern the glioblastoma tumor initiating cell state [28]. ZFHX4 is also found as a prognostic factor for ovarian serous cystadenocarcinoma, esophageal cancer, and lung adenocarcinoma. Understanding the role of pivotal genetic variations in CRC cancer development and growth is a promising direction for future research.

CRC is a highly heterogeneous disease, and clinically similar tumors with similar pathology differ significantly in terms of treatment response and patient survival. Pathologic staging is critical to the efficacy of biological therapy for CRC, and the traditional classification of CRC does not fully reflect tumor heterogeneity and cannot accommodate the needs of modern cancer therapy. The concept of molecular classification is to shift the classification of tumors from morphological to molecular characteristics through comprehensive molecular analysis techniques. Afterward, with the in-depth study of the mechanism at the molecular level and the advancement of sequencing technology, the molecular typing methods of tumors have been expanded from relying on single or few markers detection to the stage of spectroscopic typing, which has led more researchers to perform molecular typing of CRC. However, there is no uniform standard for molecular typing of CRC for now. After analyzing 18 different CRC gene expression datasets, the International CRC subtyping collaborative (CRCSC) established 4 CRC molecular signature consensus subgroups (CMS) in 2015, including CMS1, CMS2, CMS3, and CMS4 [29]. Among them, CMS1 (MSI immune subtype) is distinguished by MSI, BRAF mutation, high CpG island methylator phenotype (CIMP), immune infiltration, and poor survival; CMS2 (typical) has a high somatic copy number alterations (SCNA) level; CMS3 (metabolic) is characterized by low SCNA and CIMP, KRAS mutation, and metabolic dysregulation; CMS4 (mesenchymal) is characterized by high SCNA, stromal infiltration, TGF activation, angiogenesis, and short survival. CMS typing is currently considered to be the most convincing method for colorectal

cancer staging, and many researchers have conducted studies on CRC-targeted therapy based on this method. In this study, we identified the CRC subtype associated with the PFS. As shown in Figure 5(b), subtype C1 had the longest PFS with a median time of 8.2 years, while subtypes C2 and C3 had 4.1 and 2.7 years PFS, respectively. Patients' clinicopathological staging was also related to the CRC subtype that we identified.

Following the determination of the three subtypes based on the expression of CRC-related mutated genes, the immune infiltration of the three groups was evaluated by using the CIBERSORT method. We demonstrated that B cell native, T cell CD8+, T cell CD4+ memory activated, T cell gamma delta, NK cell resting, macrophage M0, macrophage M2, myeloid dendritic cell activated, mast cell activated, and mast cell resting had differences among the three groups. According to the findings, the three subgroups classified by 22 somatically significantly mutated genes had a high capacity to differentiate patients with different immune statuses, which is helpful for the prediction of immunotherapy response of CRC patients.

This study still has some limitations. First, despite the data from CRC patients used in this study being extracted from TCGA, the sample size was still small; second, despite the obvious clinical significance of the newly proposed subtypes, little is known about their underlying mechanism. As a result, we must investigate the molecular mechanisms of the three subtypes. Third, there is no validation of the functions of hub genes.

Finally, the current investigation confirmed the predictive significance of somatically altered genes and offered a novel genomic categorization with clinical relevance. This discovery presented a foundation for CRC research and molecular classification of CRC types to guide precision therapy by interpreting genomic data.

Abbreviations

CRC: Colorectal cancer
WES: Whole exosome sequencing
DEGs: Differentially expressed genes
PFS: Progression-free survival
DMMR: Deficient mismatch repair
MSI-H: Microsatellite instability-high
MSS: Microsatellite stable
pMMR: Mismatch repair proficient
FAP: Familial adenomatous polyposis
CMS: CRC molecular signature consensus subgroups
TMB: Tumor burden
CIMP: CpG island methylator phenotype
SCNA: Somatic copy number alterations.

Data Availability

The data used to support the findings of this study are available from the corresponding author upon request.

Conflicts of Interest

The authors declare that they have no conflicts of interest.

Authors' Contributions

He Y. S. and Huang S. Y. designed the study, interpreted data, and drafted the manuscript. Dai X. and Chen Y. Y. analyzed data and revised for important intellectual content. Yongshan He, Xuan Dai, and Shiyong Huang contributed equally to this work.

References

[1] H. Chen, X. Zheng, X. Zong et al., "Metabolic syndrome, metabolic comorbid conditions and risk of early-onset colorectal cancer," *Gut*, vol. 70, no. 6, pp. 1147–1154, 2021.

[2] Y. Xi and P. Xu, "Global colorectal cancer burden in 2020 and projections to 2040," *Translational Oncology*, vol. 14, no. 10, Article ID 101174, 2021.

[3] S. Filip, V. Vymetalkova, J. Petera et al., "Distant metastasis in colorectal cancer patients-do we have new predicting clinicopathological and molecular biomarkers? a comprehensive review," *International Journal of Molecular Sciences*, vol. 21, no. 15, p. 5255, 2020.

[4] G. Golshani and Y. Zhang, "Advances in immunotherapy for colorectal cancer: a review," *Therapeutic Advances in Gastroenterology*, vol. 13, Article ID 175628482091752, 2020.

[5] H. Gonzalez, C. Hagerling, and Z. Werb, "Roles of the immune system in cancer: from tumor initiation to metastatic progression," *Genes and Development*, vol. 32, no. 19-20, pp. 1267–1284, 2018.

[6] C. L. Ventola, "Cancer immunotherapy, part 2: efficacy, safety, and other clinical considerations," *Pharmacy and Therapeutics*, vol. 42, no. 7, pp. 452–463, 2017.

[7] A. Relecom, M. Merhi, V. Inchakalody et al., "Emerging dynamics pathways of response and resistance to PD-1 and CTLA-4 blockade: tackling uncertainty by confronting complexity," *Journal of Experimental & Clinical Cancer Research*, vol. 40, no. 1, p. 74, 2021.

[8] A. F. Oliveira, L. Bretes, and I. Furtado, "Review of PD-1/PD-L1 inhibitors in metastatic dMMR/MSI-H colorectal cancer," *Frontiers in Oncology*, vol. 9, p. 396, 2019.

[9] H. Chen, J. Wu, L. Lu et al., "Identification of hub genes associated with immune infiltration and predict prognosis in hepatocellular carcinoma via bioinformatics approaches," *Frontiers in Genetics*, vol. 11, Article ID 575762, 2020.

[10] M. D. Wilkerson and D. N. Hayes, "Consensusclusterplus: a class discovery tool with confidence assessments and item tracking," *Bioinformatics*, vol. 26, no. 12, pp. 1572-1573, 2010.

[11] Q. Liu, Y. Fang, and J. Wang, "Estimate algorithm is not appropriate for inferring tumor purity and stromal and immune cell admixture in hematopoietic or stromal tumors," *Cancer Immunology Immunotherapy*, vol. 69, no. 6, pp. 1153-1154, 2020.

[12] T. Li, J. Fan, B. Wang et al., "TIMER: a web server for comprehensive analysis of tumor-infiltrating immune cells," *Cancer Research*, vol. 77, no. 21, pp. e108–e110, 2017.

[13] J. Chen, "The cell-cycle arrest and apoptotic functions of p53 in tumor initiation and progression," *Cold Spring Harb Perspect Med*, vol. 6, no. 3, Article ID a026104, 2016.

[14] S. Jancik, J. Drabek, D. Radzioch, and M. Hajduch, "Clinical relevance of KRAS in human cancers," *Journal of Biomedicine and Biotechnology*, vol. 2010, Article ID 150960, 13 pages, 2010.

[15] S. Narayan and D. Roy, "Role of APC and DNA mismatch repair genes in the development of colorectal cancers," *Molecular Cancer*, vol. 2, no. 1, p. 41, 2003.

[16] P. J. Morin, A. B. Sparks, V. Korinek et al., "Activation of beta-catenin-Tcf signaling in colon cancer by mutations in beta-catenin or APC," *Science*, vol. 275, no. 5307, pp. 1787–1790, 1997.

[17] M. Smiech, P. Leszczynski, H. Kono, C. Wardell, and H. Taniguchi, "Emerging BRAF mutations in cancer progression and their possible effects on transcriptional networks," *Genes*, vol. 11, no. 11, p. 1342, 2020.

[18] G. Ligresti, L. Militello, L. S. Steelman et al., "PIK3CA mutations in human solid tumors: role in sensitivity to various therapeutic approaches," *Cell Cycle*, vol. 8, no. 9, pp. 1352–1358, 2009.

[19] Y. D. Chu, K. M. Kee, W. R. Lin et al., "SYNE1 exonic variant rs9479297 contributes to concurrent hepatocellular and transitional cell carcinoma double primary cancer," *Biomedicines*, vol. 9, no. 12, p. 1819, 2021.

[20] X. Xie, Y. Tang, J. Sheng et al., "Titin mutation is associated with tumor mutation burden and promotes antitumor immunity in lung squamous cell carcinoma," *Frontiers in Cell and Developmental Biology*, vol. 9, Article ID 761758, 2021.

[21] N. Lu, J. Liu, M. Xu et al., "CSMD3 is associated with tumor mutation burden and immune infiltration in ovarian cancer patients," *International Journal of General Medicine*, vol. 14, pp. 7647–7657, 2021.

[22] C. H. An, E. M. Je, N. J. Yoo, and S. H. Lee, "Frameshift mutations of cadherin genes DCHS2, CDH10 and CDH24 genes in gastric and colorectal cancers with high microsatellite instability," *Pathology and Oncology Research*, vol. 21, no. 1, pp. 181–185, 2015.

[23] Y. He, L. Cao, L. Wang, L. Liu, Y. Huang, and X. Gong, "Metformin inhibits proliferation of human thyroid cancer TPC-1 cells by decreasing LRP2 to suppress the JNK pathway," *OncoTargets and Therapy*, vol. 13, pp. 45–50, 2020.

[24] R. K. Andersen, K. Hammer, H. Hager et al., "Melanoma tumors frequently acquire LRP2 /megalin expression, which modulates melanoma cell proliferation and survival rates," *Pigment Cell Melanoma Research*, vol. 28, no. 3, pp. 267–280, 2015.

[25] Y. Wei, X. Wang, Z. Zhang et al., "Impact of NR5A2 and RYR2 3′UTR polymorphisms on the risk of breast cancer in a Chinese han population," *Breast Cancer Research and Treatment*, vol. 183, no. 1, pp. 1–8, 2020.

[26] Z. Liu, L. Liu, D. Jiao et al., "Association of RYR2 mutation with tumor mutation burden, prognosis, and antitumor immunity in patients with esophageal adenocarcinoma," *Frontiers in Genetics*, vol. 12, Article ID 669694, 2021.

[27] W. Ren, Y. Li, X. Chen et al., "RYR2 mutation in non-small cell lung cancer prolongs survival via down-regulation of DKK1 and up-regulation of GS1-115G20.1: a weighted gene Co-expression network analysis and risk prognostic models," *IET Systems Biology*, vol. 16, no. 2, pp. 43–58, 2022.

[28] Y. Chudnovsky, D. Kim, S. Zheng et al., "ZFHX4 interacts with the NuRD core member CHD4 and regulates the glioblastoma tumor-initiating cell state," *Cell Reports*, vol. 6, no. 2, pp. 313–324, 2014.

[29] J. Guinney, R. Dienstmann, X. Wang et al., "The consensus molecular subtypes of colorectal cancer," *Nature Medicine*, vol. 21, no. 11, pp. 1350–1356, 2015.

Hindawi
Genetics Research
Volume 2022, Article ID 1792977, 8 pages
https://doi.org/10.1155/2022/1792977

Research Article

The Protective Effect of *Trichosanthes kirilowii* Peel Polysaccharide on the Oxidative Damaged HepG2 and HUASMC Cells

Jinli Zhang,[1,2] **Heren Gao**,[3] **Liya Zhu**,[1,2] **Xiangyu Yuan**,[1] **Xi Yang**,[1] **Min Xu**,[1] **and Yang Yang**[1]

[1]*Anhui Vocational College of Grain Engineering, Hefei, China*
[2]*School of Food and Biological Engineering, Hefei University of Technology, Hefei, China*
[3]*Key Laboratory of Acupuncture and Moxibustion Foundation and Technology of Anhui Province, Research Institute of Acupuncture and Meridian, College of Acupuncture and Tuina, Anhui Academy of Chinese Medicine, Anhui University of Chinese Medicine, Hefei, China*

Correspondence should be addressed to Jinli Zhang; lily422416354@163.com

Received 23 May 2022; Accepted 28 June 2022; Published 18 July 2022

Academic Editor: Jianxin Shi

Background. Oxidative stress is an important cause of liver disease and atherosclerosis. Natural substances with antioxidant activity are good drugs for treating liver disease and atherosclerosis. *Trichosanthes kirilowii* Peel Polysaccharide (TKPP) can remove DPPH (2,2-Diphenyl-1-picrylhydrazyl) free radicals and hydroxyl free radicals *in vitro*, which shows antioxidant activity. Therefore, it is speculated that it can protect human hepatoma cell line (HepG2) and umbilical artery smooth muscle cell (HUASMC) against oxidative damage by hydrogen peroxide (H_2O_2). *Methods*. Oxidative damage cell models of HepG2 and HUASMC were induced by H_2O_2. HepG2 and HUASMC were divided into blank group, H_2O_2 injury group, TKPP treatment group, and glutathione (GSH) positive control group. Cell Counting Kit-8 (CCK-8) was used to detect cell viability. The level of total GSH and the amount of Nitric oxide (NO) secreted by cells were detected by specific kits. The gene and protein expressions of catalase (CAT) and superoxide dismutase (SOD) were detected by fluorescence quantitative PCR and Western Blot. *Results*. In these two kinds of cells, compared with the control group, the survival rate, total GSH level, and NO secretion, CAT and SOD gene and protein expressions were significantly decreased in the H_2O_2 damaged group. In the TKPP treatment group, the cell survival rate was significantly elevated with the increase of the polysaccharide concentration, and the total GSH level, NO secretion, CAT and SOD gene expression, and protein expression levels were also significantly increased. *Conclusion*. TKPP can improve the activities of HepG2 and HUASMC cells damaged by H_2O_2 and protect the cellular antioxidant system.

1. Introduction

According to the previous research, oxidative stress (OS) refers to a condition in which the body's oxidation and antioxidation systems are out of balance, leading to the change and damage of many intracellular molecules like DNA, RNA, lipids, and proteins [1]. OS has a detrimental impact on the body generated by free radicals and reactive oxygen species (ROS) [2], and it is thought to be related to aging [3]. Presently, many studies have shown that OS is involved in the pathogenesis of many chronic diseases [4], including liver diseases and atherosclerosis (AS) [5].

Liver disease and AS have become two seriously harmful diseases that endanger human health. Professor Ceriello introduced the common soil theory in 2004, claiming that OS was the common cause of diabetes, insulin resistance, and heart disease [6], which was proved to be an indisputable fact in 2009 [7]. Based on this theory, substances that have or promote antioxidant functions are considered potential drugs for the prevention and treatment of these diseases.

Thus, finding and developing more natural antioxidant substances or their promoting substances are of great significance to the prevention and treatment of liver diseases and AS.

Trichosanthes kirilowii Maxim is a kind of perennial climbing herb, born in the mountains and cliffs. According to Chinese traditional medicine, *Trichosanthes kirilowii* Maxim can clear heat and expectoration and nourish the lung to loosen the bowel as an ordinary medicine for a long time [8, 9]. However, its functions in many aspects like cell biology are rarely reported. Recently, it has been reported that the peel of *Trichosanthes kirilowii* Maxim is rich in polysaccharides that can scavenge DPPH free radicals and hydroxyl free radicals in vitro [10]. Therefore, we plan to investigate the role of *Trichosanthes kirilowii* Peel Polysaccharide (TKPP) in antioxidation.

In this paper, TKPP was prepared by the water extraction and alcohol precipitation method. By studying its effects on the cell activity and the secretion of antioxidant substances, such as glutathione (GSH), catalase (CAT), superoxide dismutase (SOD), and nitric oxide (NO) in human umbilical artery smooth muscle cell (HUASMC) and hepatocellular carcinoma (HCC) cell (HepG2) damaged by hydrogen peroxide (H_2O_2) oxidation, the antioxidant effect of TKPP was explored. It is hoped to provide a more theoretical basis for the exploration of therapeutic drugs for liver diseases and cardiovascular diseases.

2. Materials and Methods

2.1. Preparation of TKPP. The fresh *Trichosanthes* skin was dried, shelled, crushed, degreased in order, then added into distilled water at a ratio of 1/20 (m/v), and bathed at 80°C for 2 hours. After the water bath, the material liquid was filtered to remove slag and concentrated, and 4 times anhydrous ethanol was added into the concentrated liquid, and then the volume concentration of ethanol reached 80%. Next, the filtrate was filtered to obtain the residue, which was deproteinized by Sevag method and handled with freeze-drying to obtain TKPP.

2.2. Cell Recovery and Passage. HepG2 cells and HUASMC cells were collected from ATCC (Manassas, VA). Human umbilical artery smooth muscle cell HUASMC and hepatocellular carcinoma (HCC) cell HepG2 frozen in a liquid nitrogen tank were taken out and placed in a 37°C water bath to shake and melt. Their cell suspensions were poured into 15 mL centrifuge tubes containing 4 mL DMEM medium (Caisson, North Logan, UT, USA) with 10% FBS (Gendepot, Barker, TX, USA) and centrifuged at 1000 r/min for 3 min to discard the supernatant, then 1 mL 10% FBS and DMEM medium was added, and the suspended cells were blown with suction heads [11]. Next, these cell suspensions were removed to T25 cell culture flask with 4 mL DMEM with 10% FBS and cultured in a carbon dioxide cell incubator with 5% CO_2 at 37°C. When the cell density in these vials reached about 80%, they were passed on. The old culture medium in each bottle was removed, 5 mL sterile PBS was added for cleaning and drying, and then 1 mL trypsin was added. Cells were placed in the CO_2 cell culture box for 3 min and observed under the microscope until dispersed suspended cells were digested. Then, 4 mL DMEM with 10% FBS was poured into the culture bottle to terminate trypsin action. The suspension in each bottle was centrifuged at 1000 r/min for 3 min in the centrifuge tube. After discarding the supernatant, 1 mL DMEM with 10% FBS was added, and the suspended cells were gently blown. Next, the required number of cells was added to each cell culture flask, and then DMEM containing 10% FBS was added to make the total volume of the culture medium in each flask become 5 mL. After gently shaking the medium evenly, cell culture was continued in CO_2 cell culture box with 5% CO_2 at 37°C.

2.3. Cell Viability Detection. Cell viability assay was performed using CCK-8 kit (Dojindo, Shanghai, China). When the density of the above two cells reached about 80%, the culture bottles were taken out, and the suspension cells were achieved by the same operation as the above. The cell concentration was adjusted to 4×10^4 cells/mL, and 100 μ L of seeds was absorbed into the 96-well plate for 4×10^3 cells/well. After gentle shaking, the cells were incubated overnight in a CO_2 cell incubator at 37°C. On the next day, 96-well plates were taken out, and these cells were divided into the blank group (without TKPP and H_2O_2), H_2O_2 group (negative control group, without TKPP, but with H_2O_2), GSH positive control group (with GSH and H_2O_2), and TKPP experimental group (with TKPP and H_2O_2). In the TKPP experimental group, five concentrations of 0.625 mg/mL, 1.25 mg/mL, 2.5 mg/mL, 5 mg/mL, and 10 mg/mL were set. 2 μ·L double steam water was added to the pore plates of both the blank and H_2O_2 groups, and 2 μ·L 1 mmol/L GSH solution to the pore plates of the GSH positive control group. In TKPP experimental group, 2 μ·L of 0.625 mg/mL, 1.25 mg/mL, 2.5 mg/mL, 5 mg/mL, and 10 mg/mL TKPP solutions were added into the cell plate, respectively. The cells of the above treatment groups were placed in the CO_2 cell culture box and incubated at 37°C for 24 hours. Then, the 96-well plates were taken out, and 2 μ L of 300 μ·mol/L H_2O_2 was added to all groups except the blank group and then incubated in a CO_2 cell incubator for 4 hours. After that, the supernatant was removed, and 100 μ·L DMEM with 10% FBS was added to each well, and 10 μ·L CCK-8 solution was supplemented into each well. The cells were placed in a CO_2 cell culture box for incubation for 2 hours. Finally, a microplate reader (BioTek microplate reader) was applied to measure the optical density (OD) values at 450 nm, and the data were analyzed and processed with Graphpad Prism software.

2.4. Total Detection of GSH Level and NO Secretion. HepG2 and HUASMC cells were cultured at 37°C for 24 hours in a 6-well plate with 6×10^4 cells/well. They were still divided into blank group, H_2O_2 group (negative control group), GSH positive control group, and TKPP experimental group. The concentration of TKPP in the experimental group was 10 mg/mL. Cells of each group were

treated according to the method in 2.3, after that, the medium was removed. Then, cells were washed with PBS twice, and 100 μ·L cell lysate was added to each well. The cells and cell lysate were placed on ice for 10 min, collected into a centrifugal tube with a cell scraper, and centrifuged at 12000 r/min for 15 min at 4°C. Also, the supernatant was removed. Finally, the total GSH content of each well was determined according to GSH kit procedure (Sigma), and NO detection kit (Beyotime, Nanjing, China) was used to detect the content of NO in the old cell culture medium removed above. The above data were analyzed and processed by Graphpad Prism software.

2.5. RNA Extraction and Quantitative PCR. HepG2 and HUASMC cells were cultured at 37°C for 24 h in a 6-well plate with 6×10^4 cells/well. They were also divided into blank group, H_2O_2 group (negative control group), GSH positive control group, and TKPP experimental group, in which 10 mg/mL TKPP concentration was used in TKPP experimental group. Cell treatment in each group was the same as that in 2.3. Then, the culture medium was removed, and cells were washed with PBS twice, 100 μ·L Trizol lysis solution (Invitrogen) was added to each well, and cells were placed on ice for 10 min. The total RNA was extracted according to RNA extraction kit, and its OD260/OD280 and concentration were determined by UV spectrophotometer. If the OD260/OD280 size is between 1.8 and 2.0, RNA purity is considered to meet the requirements. Then, the concentration was adjusted to 50 μ·g/L, and the mRNA relative expression levels of CAT and SOD were determined by real-time PCR after reverse transcription with 10 μ·L reverse transcription reaction system. Reaction conditions were as follows: predenaturation at 95°C for 3 min, denaturation at 95°C for 5 s; annealing at 60°C for 30 s; extending 60°C for 30 s. With GAPDH as an internal reference, PCR primer sequences of each group were shown in Table 1. Relative expression levels of each group were calculated by $2^{-\triangle\triangle Ct}$ method.

2.6. Western Blot (WB) Assay. Cells were plated in 6-well plates with 6×10^4 cells/well and 2 mL culture medium, respectively, and cultured in a cell incubator at 37°C for 24 hours, divided into blank group, H_2O_2 group (negative control group), GSH positive control group, and TKPP experimental group. As in 2.3, 300 μ·L RIPA cell lysis solution (adding protease inhibitor) was added to each well for ice lysis for 10 min. The lysates were collected and centrifuged at 12000 r/min at 4°C for 10 min, and the supernatant was discarded. Their protein concentrations were determined by BCA method, and then all proteins were quantified to the same concentration. Then, samples were mixed with the loading buffer at a ratio of 1/4, boiled for 10 min, and stored at −20°C. SDS-PAGE electrophoresis was carried out by adding samples with equal amounts of protein to each well. After the electrophoresis, these membranes were transferred by semidry method. The required membrane transfer current and time were determined by membrane area and relative molecular weight of protein. After membrane transfer, they were rinsed with PBS for 5 min and then sealed with PBST containing 5% bovine serum albumin at room temperature for 3 hours. Then, they were rinsed 3 times with PBST on a decolorizing shaker for 10 min each, and after that, they were also rinsed with PBST 3 times, 10 min each time. Next, membranes were incubated in secondary antibody diluent at room temperature for 1 hour and rinsed 3 times with PBST for 10 min each time. These membranes were then colored and imaged by ECL chemiluminescence, and the gray level of the bands was analyzed in Image *J*.

2.7. Statistical Analysis. At least three parallel samples were used for the experimental data, and the data results were displayed as mean ± standard deviation. Statistical analysis was conducted by Graphpad Prism (GraphPad Prism software, Inc., California, USA). *represents $P < 0.05$, $^{**}P < 0.01$, $^{***}P < 0.001$, and $^{****}P < 0.0001$.

3. Results

3.1. Different Concentrations of TKPP on Cell Viability. To determine the protective effect of TKPP with different concentrations on oxidative-damaged cells, cell viability was measured with CCK-8. As seen in Figure 1(a) and 1(b), in HepG2 and HUASMC cells, compared with the blank group, the OD value of cells in the H_2O_2 group was significantly decreased, suggesting that the oxidative damage cell model was successfully constructed. In GSH group, cell viability was all elevated after adding GSH in the H_2O_2 group. Moreover, the addition of TKPP could also elevate cell activity in the H_2O_2 group, and the efficiency increased with the increase of TKPP concentration. In this experiment, 10 mg/mL TKPP was the best, and it made cell activity even higher than that of the GSH positive control group. Therefore, 10 mg/mL of TKPP was used in subsequent experimental groups.

In HepG2 and HUASMC cells, the concentration of total GSH decreased significantly in the H_2O_2 group compared with the blank group, while the level of total GSH increased significantly in the TKPP group supplemented with 10 mg/mL TKPP. Moreover, the total GSH level of the TKPP group was higher than that of the GSH positive control group (Figure 2(a)). Therefore, we concluded that TKPP effectively increased the levels of total GSH in H_2O_2-damaged cells, and it could promote the antioxidant effect in cells.

3.2. TKPP Could Effectively Promote the Secretion of NO in H_2O_2-Damaged HepG2 and HUASMC Cells. Next, we observed the concentrations of NO in different groups in HepG2 and HUASMC cells to detect the effect of TKPP on NO secretion. It was found that the secretion of NO in the H_2O_2 group was significantly decreased compared with the blank group, while the secretion of NO in the TKPP group was significantly increased, and its level was close to that of the GSH positive control group (Figure 2(b)). Thus, we found that TKPP could effectively promote the secretion of NO in H_2O_2-damaged HepG2 and HUASMC cells and might resist cell apoptosis, according to NO characteristics [12].

Table 1: Real-time PCR primer sequences.

Gene	Forward (5′–3′)	Reverse (5′-3′)
GAPDH	GGAGCGAGATCCCTCCAAAAT	GGCTGTTGTCATACTTCTCATGG
CAT	TAAGACTGACCAGGGCATC	CAACCTTGGTGAGATCGAA
SOD	GAGATGTTACACGCCCAGATAGC	AATCCCCAGCAGTGGAATAAGG

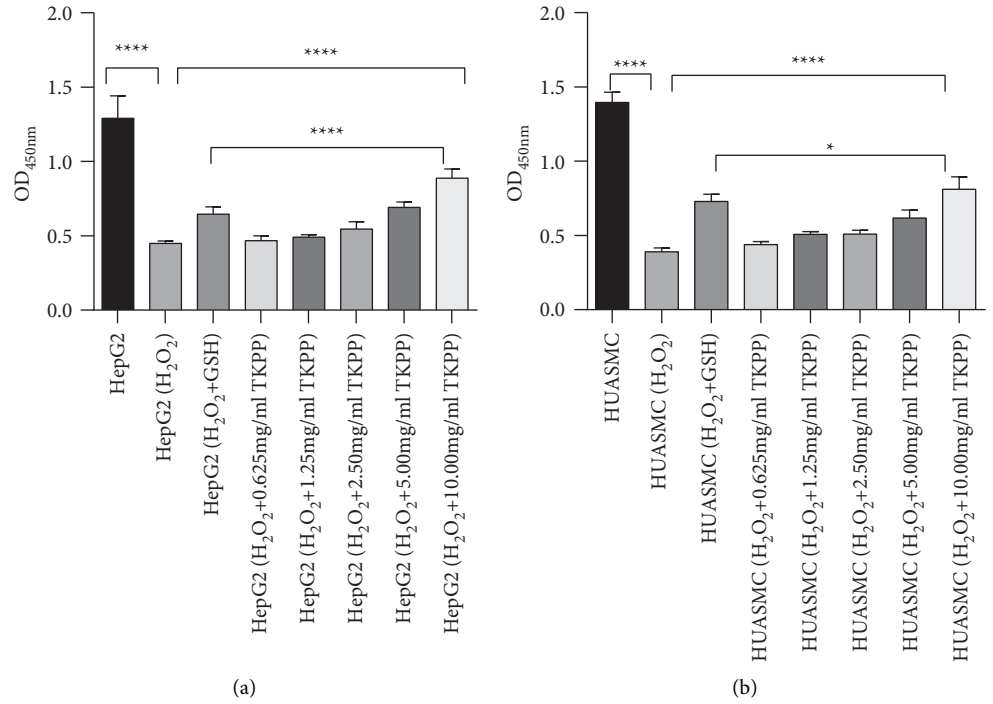

Figure 1: Effects of TKPP with different concentrations on HepG2 (a) and HUASMC (b) cell viability. $^{*}P < 0.05$, $^{****}P < 0.0001$. TKPP could promote the GSH level in H_2O_2-damaged cells.

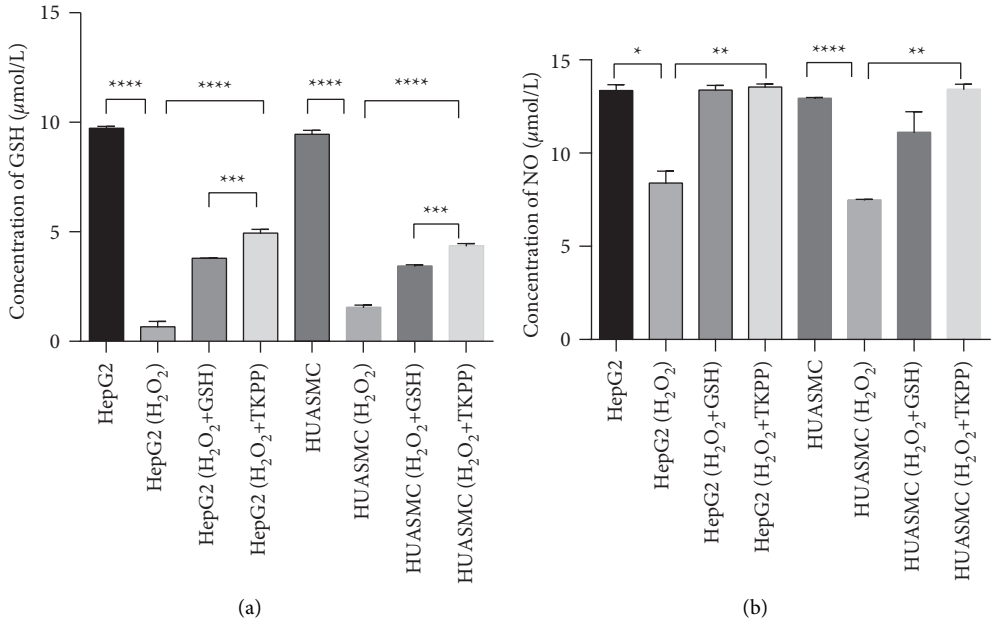

Figure 2: The expression detection of GSH and NO in different groups. (a) The level of GSH in oxidized HepG2 and HUASMC cells. (b) The NO secretion in oxidized HepG2 and HUASMC cells. $^{*}P < 0.05$, $^{**}P < 0.01$, $^{***}P < 0.001$, and $^{****}P < 0.0001$.

3.3. TKPP Could Enhance the Expressions of Antioxidant Enzymes in HepG2 and HUASMC Cells Damaged by H_2O_2. To evaluate the effects of TKPP on the antioxidant enzymes in oxidative-damaged HepG2 and HUASMC cells, the levels of CAT and SOD in each group were analyzed by fluorescence quantitative PCR. In both cells, the expressions of CAT and SOD in the H_2O_2 group were significantly lower than those in the blank group, while the expression levels of CAT and SOD in the TKPP group were significantly increased when 10 mg/mL TKPP was added. In HepG2 cells, the level of CAT in TKPP group was similar to that in the GSH positive control group, while the level of SOD was much higher. In HUASMC cells, the levels of CAT and SOD genes in TKPP group were also much higher than those in the GSH positive control group (Figure 3(a) and 3(b)). Based on the above findings, TKPP could effectively promote the expressions of antioxidant enzymes in HepG2 and HUASMC cells damaged by H_2O_2, thus enhancing the antioxidant effect of cells.

In order to determine the effect of TKPP on the expression of antioxidant enzyme proteins in oxidative-damaged HepG2 and HUASMC cells, the expression of CAT and SOD proteins in each group was analyzed by WB. In both cells, the levels of CAT and SOD proteins in the H_2O_2 group were lower than those in the blank group, while in the TKPP group, with the addition of 10 mg/mL TKPP, they were significantly increased, close to or higher than that in the GSH positive control group (Figure 4(a)–4(c)). Thus, polysaccharides from *Trichosanthes kirilowii* Maxim could significantly promote the protein expression of antioxidant enzymes in cells damaged by H_2O_2 oxidation.

4. Discussion

In biological cells, there exist two antioxidant systems (enzyme and nonenzymatic antioxidant systems) to maintain the balance between oxidation and antioxidation [13]. Enzymatic antioxidants include SOD, CAT, and glutathione peroxidase (GPx); the first two are the most common antioxidant enzymes in living organisms [14]. SOD is the first defense line against oxygen free radicals, which can promote the superoxide into oxygen gas and hydrogen peroxide [15]. When exposed to OS, CAT can be neutralized by the decomposition of hydrogen peroxide into molecular oxygen and water [16]. The expressions of antioxidant enzymes (CAT, SOD, and GPx) can be detected to judge the condition of OS and antioxidant effect in cells.

The nonenzymatic antioxidant system contains GSH, coenzyme *Q*, uric acid, metallothionein, L-carnitine, and so on [17]. These antioxidants can neutralize free radicals and ROS, reduce cell damage caused by them, and prevent oxidative damage to cells and tissues [14]. As a small molecule peptide of three amino acids, GSH is the main reservoir of intracellular sulfo groups and a reducing agent to protect the OS-damaged tissues [18]; thus, it can be used as an indicator of redox potential and the ability of cells to prevent OS. Moreover, it also participates in the detoxification of exogenous compounds and the metabolism of various intracellular compounds in vivo [19]. Herein, we detected the levels of GSH, CAT, and SOD in oxidative-damaged cells to observe the antioxidative efficiency of TKPP. The results demonstrated that TKPP could promote their expressions and possess a good antioxidative ability.

NO is usually catalyzed by nitric oxide synthase (NOS) to produce L-arginine, which exists in various organs like the liver, lung, and blood vessels [20]. It has been reported to have an important role in cell homeostasis, neurotransmission, central nervous system neuroregulation, immune response, signal transduction, cell proliferation, and apoptosis and can effectively combat OS [21]. NO can combine with hydroxyl radical and superoxide anion radical to detoxify as an antioxidant role [22]. In addition, it mediates the expression of cellular protective genes, such as heat shock protein HSP70, to prevent liver cells from the apoptosis induced by TNFα, oxygen ions, and nitrite ions [23]. Besides, NO can also indirectly block the activation of the Caspase family by changing mitochondrial permeability, thereby preventing the Caspase activation and blocking the apoptosis signaling, thus inhibiting the cell apoptosis [12]. In this study, we measured the secretion of NO in different groups and found that TKPP could promote NO expression. So, we suspected that TKPP might have an inhibitory function for cell apoptosis, which needed further investigation.

H_2O_2 can cause cell peroxidation damage by producing oxygen free radicals or hydroxyl free radicals [24, 25]. Previously, many reports chose the hydrogen peroxide-induced OS cell model to comprehensively evaluate the antioxidant activity of plant chemical components or extracts and elaborate the antioxidant mechanism accordingly [26]. Based on this foundation, we also chose H_2O_2 to prepare the oxidation-damaged model. As for the experimental cells, metabolic enzymes in HepG2 cells remain relatively stable, and phenotypes and inner parts do not change with the increase of passage times [27]. It contains biotransforming metabolic enzymes of the same origin as human normal liver parenchyma cells [28] and is often used as an ideal cell line for *in vitro* hepatocyte metabolism and genetic testing [29]. In addition, oxidative damage and abnormal apoptosis of vascular smooth muscle cells can promote the formation of atherosclerotic plaques, thus promoting the development of AS [30, 31]. Therefore, HepG2 and HUASMC cells were selected for oxidative damage experiments to study the antioxidant protection of TKPP.

In our functional experiments, we firstly determined the best concentration of TKPP in the oxidation-damaged cells, and 10 mg/mL showed the best promotion for cell viability. Next, cells were divided into blank group, H_2O_2 group, GSH positive control group, and TKPP experimental groups, and the expressions of GSH, NO, SOD, and CAT were detected, respectively. Next, WB was applied to measure the protein expressions of CAT and SOD. All the results showed that TKPP was an antioxidative promotor in oxidation-damaged cells, indicating that it had a good antioxidative effect in cells. In other words, it offers a direction for new drug research and development in many diseases, including liver diseases and AS.

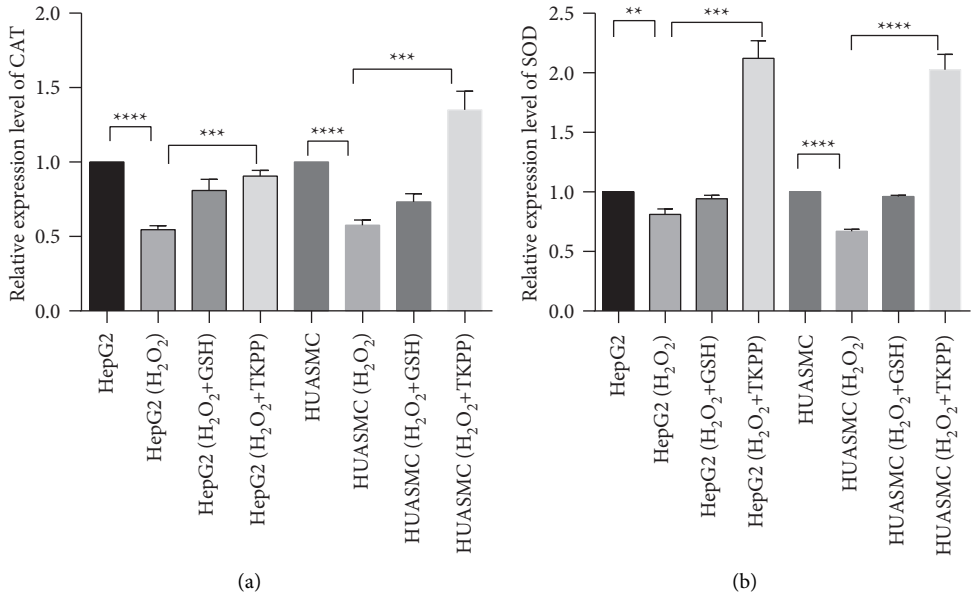

Figure 3: Effects of TKPP on the expression of CAT (a) and SOD (b) in oxidative-damaged HepG2 and HUASMC cells. $^{**}P < 0.01$, $^{***}P < 0.001$, and $^{****}P < 0.0001$. Protein expression detection of CAT and SOD in TKPP group.

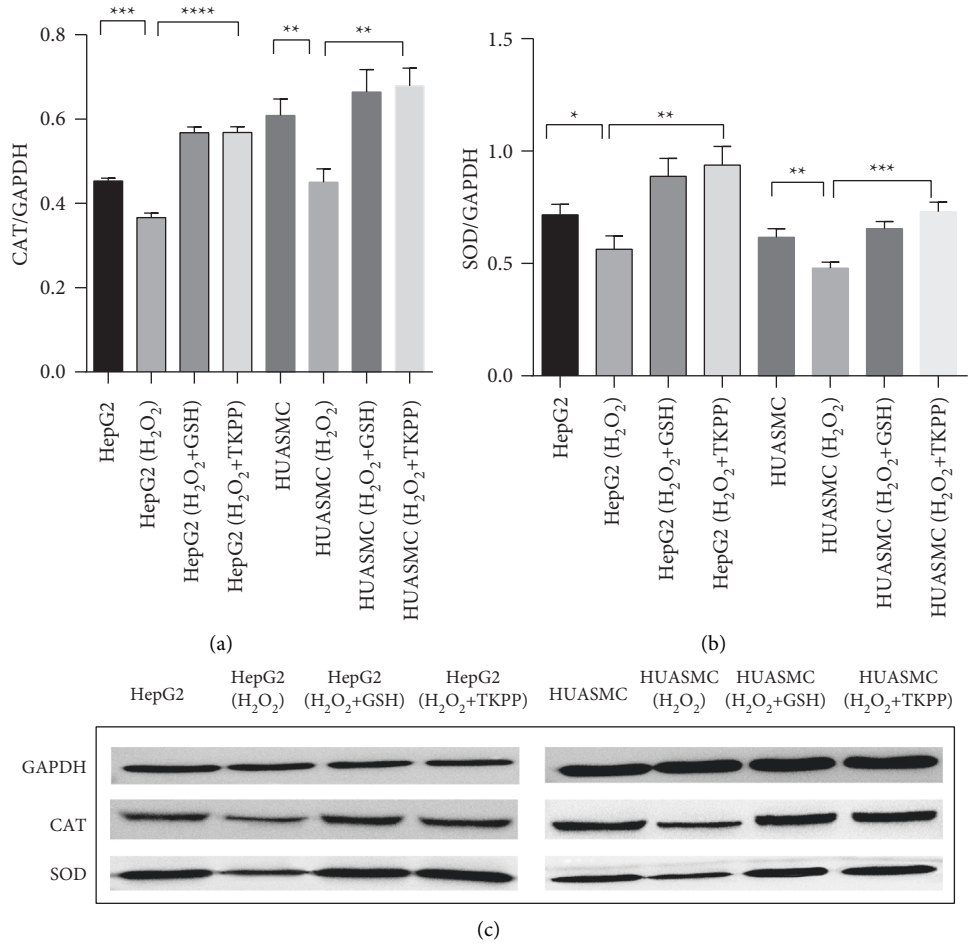

Figure 4: Protein expression detection of CAT and SOD in TKPP group. (a) Band intensity of CAT protein expressions in each group. (b) Band intensity of SOD protein expressions in each group. (c) Immunoblotting of CAT and SOD proteins in each group. $^{*}P < 0.05$, $^{**}P < 0.01$, $^{***}P < 0.001$, and $^{****}P < 0.0001$.

5. Conclusion

In summary, TKPP can effectively promote the antioxidant effect of human hepatoma cell line HepG2 and human umbilical artery smooth muscle cells HUASMC and resist oxidative damage and apoptosis induced by H_2O_2 by enhancing the expressions of GSH, CAT, and SOD in the natural antioxidant system and the level of NO secretion. Therefore, TKPP has the potential to be the therapeutic target in the prevention and treatment of liver diseases and AS, which is expected to be applied in the clinic in the future.

Data Availability

The datasets used during the present study are available from the corresponding author upon reasonable request.

Conflicts of Interest

The authors declare that they have no conflicts of interest to report regarding the present study.

Authors' Contributions

Study conception and design were done by Jinli Zhang; data collection was done by Heren Gao and Liya Zhu; analysis and interpretation of results were perfromed by Xiangyu Yuan and Xi Yang; draft manuscript was prepared by Min Xu and Yang Yang. All authors reviewed the results and approved the final version of the manuscript.

Acknowledgments

This work is supported by the Natural Science Foundation of Colleges and Universities of Anhui Province (Grant number: KJ2019A1267); the Outstanding Top-Notch Talents Training Program of Anhui Provincial Department of Education (Grant number: gxgnfx2020179) and the Natural Science Foundation of Anhui Province (Grant number: 1908085QH341).

References

[1] S. Venus, M. Teresa, S. Rosa, P. Rosanna, K. Hiroshi, and E. L. Matilde, "Oxidative stress and cancer: an overview," *Ageing Research Reviews*, vol. 12, 2013.

[2] K. Jakubczyk, K. Dec, J. Kałduńska, D. Kawczuga, J. Kochman, and K. Janda, "Reactive oxygen species - sources, functions, oxidative damage," *Polski Merkuriusz Lekarski: Organ Polskiego Towarzystwa Lekarskiego*, vol. 48, no. 284, pp. 124–127, 2020.

[3] Y. Gu, J. Han, C. Jiang, and Y. Zhang, "Biomarkers, oxidative stress and autophagy in skin aging," *Ageing Research Reviews*, vol. 59, Article ID 101036, 2020.

[4] R. S. Sohal, "Oxidative stress hypothesis of aging," *Free Radical Biology and Medicine*, vol. 33, no. 5, pp. 573-574, 2002.

[5] !!! INVALID CITATION !!! (Bhattacharyya et al., 2014; Chen et al., 2015; Nathan and Cunningham-Bussel, 2013).

[6] A. Ceriello and E. Motz, "Is oxidative stress the pathogenic mechanism underlying insulin resistance, diabetes, and cardiovascular disease? The common soil hypothesis revisited," *Arteriosclerosis, Thrombosis, and Vascular Biology*, vol. 24, no. 5, pp. 816–823, 2004.

[7] R. Retnakaran and B. R. Shah, "Mild glucose intolerance in pregnancy and risk of cardiovascular disease: a population-based cohort study," *Canadian Medical Association Journal*, vol. 181, no. 6-7, pp. 371–376, 2009.

[8] H. Zhao and L. Song, "TKP, a serine protease from trichosanthes kirilowii, inhibits cell proliferation by blocking aerobic glycolysis in hepatocellular carcinoma cells," *Nutrition and Cancer*, vol. 74, no. 1, pp. 333–345, 2022.

[9] X. Lei, N. Li, Z. Bai et al., "Chemical constituent from the peel of Trichosanthes kirilowii Maxim and their NF-κB inhibitory activity," *Natural Product Research*, vol. 35, no. 23, pp. 5132–5137, 2021.

[10] !!! INVALID CITATION !!! (Chen et al., 2016; Chu and Zhang, 2018; Sunhre et al., 2020).

[11] !!! INVALID CITATION !!! (Acito et al., 2020; Ulrich-Merzenich et al., 2002).

[12] W. Wu, X. Gao, X. Xu et al., "Saponin-rich fraction from Clematis chinensis Osbeck roots protects rabbit chondrocytes against nitric oxide-induced apoptosis via preventing mitochondria impairment and caspase-3 activation," *Cytotechnology*, vol. 65, no. 2, pp. 287–295, 2013.

[13] E. Niki, "Assessment of antioxidant capacity in vitro and in vivo," *Free Radical Biology and Medicine*, vol. 49, no. 4, pp. 503–515, 2010.

[14] I. Mirończuk-Chodakowska, A. M. Witkowska, and M. E. Zujko, "Endogenous non-enzymatic antioxidants in the human body," *Advances in Medical Sciences*, vol. 63, no. 1, pp. 68–78, 2018.

[15] D. V. Ratnam, D. D. Ankola, V. Bhardwaj, D. K. Sahana, and M. N. V. R. Kumar, "Role of antioxidants in prophylaxis and therapy: a pharmaceutical perspective," *Journal of Controlled Release*, vol. 113, no. 3, pp. 189–207, 2006.

[16] L. He, T. He, S. Farrar, L. Ji, T. Liu, and X. Ma, "Antioxidants maintain cellular redox homeostasis by elimination of reactive oxygen species," *Cellular Physiology and Biochemistry*, vol. 44, no. 2, pp. 532–553, 2017.

[17] M. E. Lönn, J. M. Dennis, and R. Stocker, "Actions of "antioxidants" in the protection against atherosclerosis," *Free Radical Biology and Medicine*, vol. 53, no. 4, pp. 863–884, 2012.

[18] P. Ahmad, C. A. Jaleel, M. M. Azooz, and G. Nabi, "Generation of ROS and non-enzymatic antioxidants during abiotic stress in plants," *Botany Research International*, vol. 2, no. 1, pp. 11–20, 2009.

[19] J. P. E. Spencer, G. G. C. Kuhnle, R. J. Williams, and C. Rice-Evans, "Intracellular metabolism and bioactivity of quercetin and its in vivo metabolites," *Biochemical Journal*, vol. 372, no. 1, pp. 173–181, 2003.

[20] Y. Y. Ji, Y. J. Ma, and J. W. Wang, "Cytoprotective role of nitric oxide in HepG2 cell apoptosis induced by hypocrellin B photodynamic treatment," *Journal of Photochemistry and Photobiology B: Biology*, vol. 163, pp. 366–373, 2016.

[21] J. R. Tejedo, R. Tapia-Limonchi, S. Mora-Castilla et al., "Low concentrations of nitric oxide delay the differentiation of embryonic stem cells and promote their survival," *Cell Death & Disease*, vol. 1, no. 10, p. e80, 2010.

[22] J. C. Wong and R. R. Fiscus, "Essential roles of the nitric oxide (no)/cGMP/protein kinase G type-Iα (PKG-Iα) signaling pathway and the atrial natriuretic peptide (ANP)/cGMP/PKG-Iα autocrine loop in promoting proliferation and cell survival of OP9 bone marrow stromal cells," *Journal of Cellular Biochemistry*, vol. 112, no. 3, pp. 829–839, 2011.

[23] !!! INVALID CITATION !!! (Kim et al., 1997; Sidahmed et al., 2013).

[24] H. Wang, J. Liu, X. Liu, and Z. Liu, "Protective effects of blueberry against hydrogen peroxide-induced oxidative stress in HEPG2 cells," *British Food Journal*, vol. 121, no. 11, pp. 2809–2820, 2019.

[25] M.-M. Jin, L. Zhang, H.-X. Yu, J. Meng, Z. Sun, and R. R. Lu, "Protective effect of whey protein hydrolysates on H2O2-induced PC12 cells oxidative stress via a mitochondria-mediated pathway," *Food Chemistry*, vol. 141, no. 2, pp. 847–852, 2013.

[26] !!! INVALID CITATION !!! (Bak et al., 2014; Hu et al., 2022; Su et al., 2011; Sun et al., 2022).

[27] T. Hurrell, A. A. Ellero, Z. F. Masso, and A. D. Cromarty, "Characterization and reproducibility of HepG2 hanging drop spheroids toxicology in vitro," *Toxicology in Vitro*, vol. 50, pp. 86–94, 2018.

[28] A. Lançon, N. Hanet, B. Jannin et al., "Resveratrol in human hepatoma HepG2 cells: metabolism and inducibility of detoxifying enzymes," *Drug Metabolism and Disposition*, vol. 35, no. 5, pp. 699–703, 2007.

[29] M. Štampar, J. Tomc, M. Filipič, and B. Žegura, "Development of in vitro 3D cell model from hepatocellular carcinoma (HepG2) cell line and its application for genotoxicity testing," *Archives of Toxicology*, vol. 93, no. 11, pp. 3321–3333, 2019.

[30] G. Ulrich-Merzenich, C. Metzner, B. Schiermeyer, and H. Vetter, "Vitamin C and vitamin E antagonistically modulate human vascular endothelial and smooth muscle cell DNA synthesis and proliferation," *European Journal of Nutrition*, vol. 41, no. 1, pp. 27–34, 2002.

[31] J. V. Tapia-Vieyra, B. Delgado-Coello, and J. Mas-Oliva, "Atherosclerosis and cancer; a resemblance with far-reaching implications," *Archives of Medical Research*, vol. 48, no. 1, pp. 12–26, 2017.